

Supervised deep learning prediction of the formation enthalpy of the full set of configurations in complex phases: the σ -phase as an example

Jean-Claude Crivello* and Jean-Marc Joubert

*Univ Paris Est Creteil, CNRS, ICMPE, UMR 7182,
2 rue Henri Dunant, 94320 Thiais, France*

Nataliya Sokolovska

NutriOmics, INSERM, Sorbonne University Paris, France

(Dated: November 24, 2020)

Abstract

Machine learning (ML) methods are becoming integral to scientific inquiry in numerous disciplines, such as material sciences. In this manuscript, we demonstrate how ML can be used to predict several properties in solid-state chemistry, in particular the heat of formation of a given complex crystallographic phase (here the σ -phase, $tP30$, $D8_b$). Based on an independent and unprecedented large first principles dataset containing about 10,000 σ -compounds with $n = 14$ different elements, we used a supervised learning approach, to predict all the \sim 500,000 possible configurations within a mean absolute error of 23 meV/at (\sim 2 kJ.mol $^{-1}$) on the heat of formation and \sim 0.06 Å on the tetragonal cell parameters. We showed that neural network regression algorithms provide a significant improvement in accuracy of the predicted output compared to traditional regression techniques. Adding descriptors having physical nature (atomic radius, number of valence electrons) improves the learning precision. Based on our analysis, the training database composed of the only binary-compositions plays a major role in predicting the higher degree system configurations. Our result opens a broad avenue to efficient high-throughput investigations of the combinatorial binary calculation for multicomponent prediction of a complex phase.

I. INTRODUCTION

The statistical machine learning (ML) is the art to construct statistical models from observational data. Machine learning, being a domain of artificial intelligence, revolutionised research in many fields (image processing, natural language, speech processing, biology and medicine, *etc.*)^{1–3}, and the number of publications introducing new statistical methods has exploded within the last decades. Strange but true that the applications of the machine learning methods to the material sciences, although more and more visible,⁴ are still falling behind compared to other applications. Among the successful applications of the ML to the materials science, is automatic extraction of predictive models from existing materials data,^{5,6} and discovery of new class of promising materials or composition, such as the fashionable high entropy alloys (HEA)^{7–10}. So far, materials scientists have used ML to build predictive models for a few applications such as to predict heat capacity,¹¹ semiconducting band gap,^{12,13} *etc.*, but also the heat of formation of inorganic compounds.^{14–17} All these recent studies have emerged with the powerful use of high-throughput calculations, such as density functional theory (DFT) impelled for large projects in the last decade (AFLOW¹⁸, OQMD¹⁸, NOMAD¹⁹ *etc.*). In fact, the increasing availability of DFT data, combined with modern data mining and ML techniques, has enabled the construction of a predictive model to replace DFT calculations and accelerate data generation.²⁰ Prediction of crystal structure is still the holy Grail in inorganic chemistry, while the component prediction is one promising approach.²¹ However, in recent work of Kim *et al.*,²² the effect of the space quality has been investigated and illustrated that ML performance can be rather poor if there are several bad (noisy) training data quite close to good candidates.²³

The contribution of the current work is two-fold: (*i*) we introduce a general high performance ML-based framework for predicting the heat of formation, corresponding to the energy scale which measures the strength of chemical bonds in a compound, where an input to the ML methods are the combinations of the elements in a given crystal structure; and (*ii*) we present and explore new original data set that we constructed and managed.

Note that heat of formation prediction was the aim of several studies and attempts, like the semi-empirical Miedema's model.²⁴ In fact, this fundamental value, called also enthalpy of formation ($\Delta_f H$ in meV) is the key parameter in thermodynamics modelling, such as in the calculation of phase diagrams (Calphad method).²⁵ We have applied the $\Delta_f H$ determi-

nation to a large combinatorial challenge, yielded by the distribution of every atom from a given space (n -base) into every s non-equivalent crystallographic sites of a given phase. This kind of description is well known in thermodynamic modelling for addressing the energy of a multicomponent and non-stoichiometric phases and is called the Compound Energy Formalism (CEF).²⁶ In CEF, each crystal site is considered as a sublattice and the distribution of every atom generates n^s unique configurations, called end-members, the $\Delta_f H$ of which has to be given to use this model.

To illustrate the efficiency of our ML framework, we investigated an important phase in the field of metallurgy: the σ -phase ($D8_b$). Its complex crystallographic structure is composed of 30 atoms in its tetragonal cell, occupying $s = 5$ distinct sites (i, j, k, l, m), as summarized in Supplementary Informations SI-A. Its features has been discussed in details.²⁷ This phase appears in many types of engineering alloys and its formation prediction requires reliable thermodynamical description. Properly, it is shown that it is important to keep a 5-sublattice model in CEF to properly describe the configuration of the σ -phase in multicomponent alloys.^{28,29} The difficulty lies in the large number of end members which must be considered in multicomponent systems. In fact, the description for a binary system (2 elements) leads to the generation of $2^5 = 32$ different ordered configurations to express, but this number rapidly increases with the degree of the system: ternary with $3^5 = 243$, quaternary with with $4^5=1024$, ... up to a real alloys with ~ 14 different elements and its $14^5 = 537,824$ configurations. Since the corresponding huge number of $\Delta_f H$ cannot be calculated by classical DFT, their prediction using ML is computationally tractable and, therefore, looks attractive and is one of the major contributions of this paper.

II. RESULTS

The results of this study – our new and original data set, ML metrics used to test the statistical methods, and the corresponding results – are described below. First, we discuss the architecture of our method, detailed later in the Methods section. Second, we demonstrate its application to the heat of formation prediction, and, finally, we report the prediction performance.

A. General-purpose method

The originality of current work is in construction of our learning database. Instead of a mishmash of massive data coming from several independent phases and from various high-throughput sources (calculated using different parameters), we built a single σ -phase oriented database with our own consistent massive DFT calculations. In addition to some additional physical parameters, the main descriptors are the combination of $n = 14$ different elements on the different $s = 5$ crystallographic sites that described the σ -phase. Among the combinatorial set (described in SI-B), a selection of data in the training set includes all the possible binary compositions (system degree $d = 2$), which represents only 0.5% of the all possible configurations. A graphical chartflow of the present methodology is given on Figure 1.

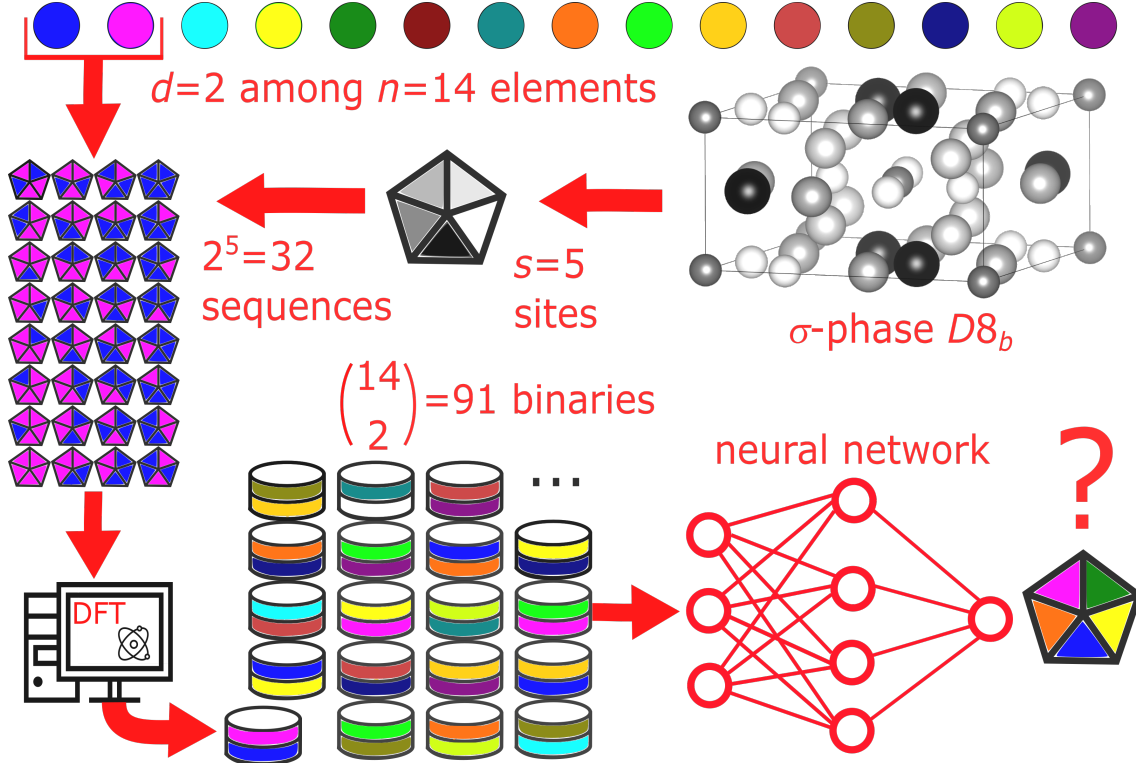


FIG. 1: Chart-flow of the methodology presented in the paper. (i) The crystal structure is summarized as a s non-equivalent sites figure; (ii) from n available elements, a given system of system degree d is selected (e.g. $d = 2$ for binary); (iii) the permutation leads to d^s unique configurations ; (iv) every configuration is calculated by DFT, forming a unit of data; (v) the stack of all $\binom{n}{d}$ units forms a learning database; then (vi) a supervised machine learning is used to predict multicomponent configurations.

B. Prediction of the heat of formation

The observations are the independent variables (from configurations X_{ijklm} of the training database with $N \simeq 10,000$ data, detailed in SI-C), and the aim of the regression analysis is to generate a statistical model that can predict a dependent variable, y_{ijklm} (the heat of formation in our case). Several regression algorithms have been investigated by choosing the best parameter to produce the most accurate generalising results. The evaluation of the prediction accuracy of a model is characterized using the coefficient of determination R^2 , the mean absolute error MAE, and the root mean squared error RMSE, given as:

$$R^2 = 1 - \frac{\sum (y_{ijklm} - \hat{y}_{ijklm})^2}{\sum (y_{ijklm} - \bar{y})^2}, \quad (1)$$

$$\text{MAE} = \frac{1}{N} \sum_{\{i,j,k,l,m\}}^N |y_{ijklm} - \hat{y}|, \quad (2)$$

$$\text{RMSE} = \sqrt{\frac{1}{N} \sum_{\{i,j,k,l,m\}}^N (y_{ijklm} - \hat{y}_{ijklm})^2}, \quad (3)$$

where \hat{y} is the predicted value based on the learned model, and \bar{y} the average value.

First, we have estimated a number of regression models from our learning database. Namely, we tested the Ridge Linear Regression, Elastic Net Linear Regression, Random Forest Regression (RFR), Multi-Layer Perceptron Regression (MPR), Gradient Boosting Machine (BBM), Support Vector Machine (SVM), K-Nearest Neighbours, Bayesian Ridge Regression, and Gaussian Process Regression (GPR). Our averaged results from 10-fold cross validation are summarized in Table I, and also shown in SI-D. Classical regression with various regularization such as LASSO (Least Absolute Shrinkage and Selection Operator), Ridge regression, or their combination, also known as Elastic Net, are not accurate enough, since the number of observations in the database is not very big. Moreover, the sparsity inducing penalties (LASSO and Elastic Net) are not very relevant to our case, since the number of parameters is quite small.

On the other hand, non-linear supervised learning methods achieve very reasonable performance. The R^2 closest to 1 are obtained with RFR, MPR, GBM and SVM regression algorithms. The associated best MAE (average from 10-fold CV) are obtained for the MPR method with 13 meV (~ 1 kJ/mol) using 3 hidden layers, each containing 500 units.

TABLE I: Cross validation scores on the complete data set (average values from 10-fold) using various machine learning methods. MAE, MSE and RMSE in meV/at (1 meV \sim 0.0965 kJ/mol), illustrated in SI-D.

Algorithm	R^2	MAE	RMSE
Ridge Linear Regression	0.45	73	110
Elastic Net Linear Regression	0.46	73	109
Random Forest Regressor (RFR)	0.89	31	56
Multi-layer Perceptron Regressor (MPR)	0.96	13	31
Gradient Boosting Machine (GBM)	0.95	19	37
Support Vector Machine Reg (SVM)	0.91	26	54
K-nearest neighbors	0.61	55	93
Bayesian Ridge Regression	0.45	73	110
Gaussian Process Regression (GPR)	0.87	30	66

C. Validation of learned models on an independent validation set

Random Forest Regression, Multi-Layer Perceptron Regression, Gradient Boosting and Support Vector Machines have shown the best performance on the data set containing 9974 inputs (our training database, SI-C). We tested these regressors on a new, previously unobserved during the training procedure, set of configurations: 1001 randomized observations among the 537,824 possible ones (testing set given in SI-E). Using MPR, the achieved accuracy of total energy, and therefore heat of formation, with a MAE of about 23 meV/at (Fig. 2) provides a very reasonable accuracy compared to other ML methods of the literature, where the standards are usually around MAE \sim 50 meV/at for systems higher than binaries.^{14,15,20,30,31}

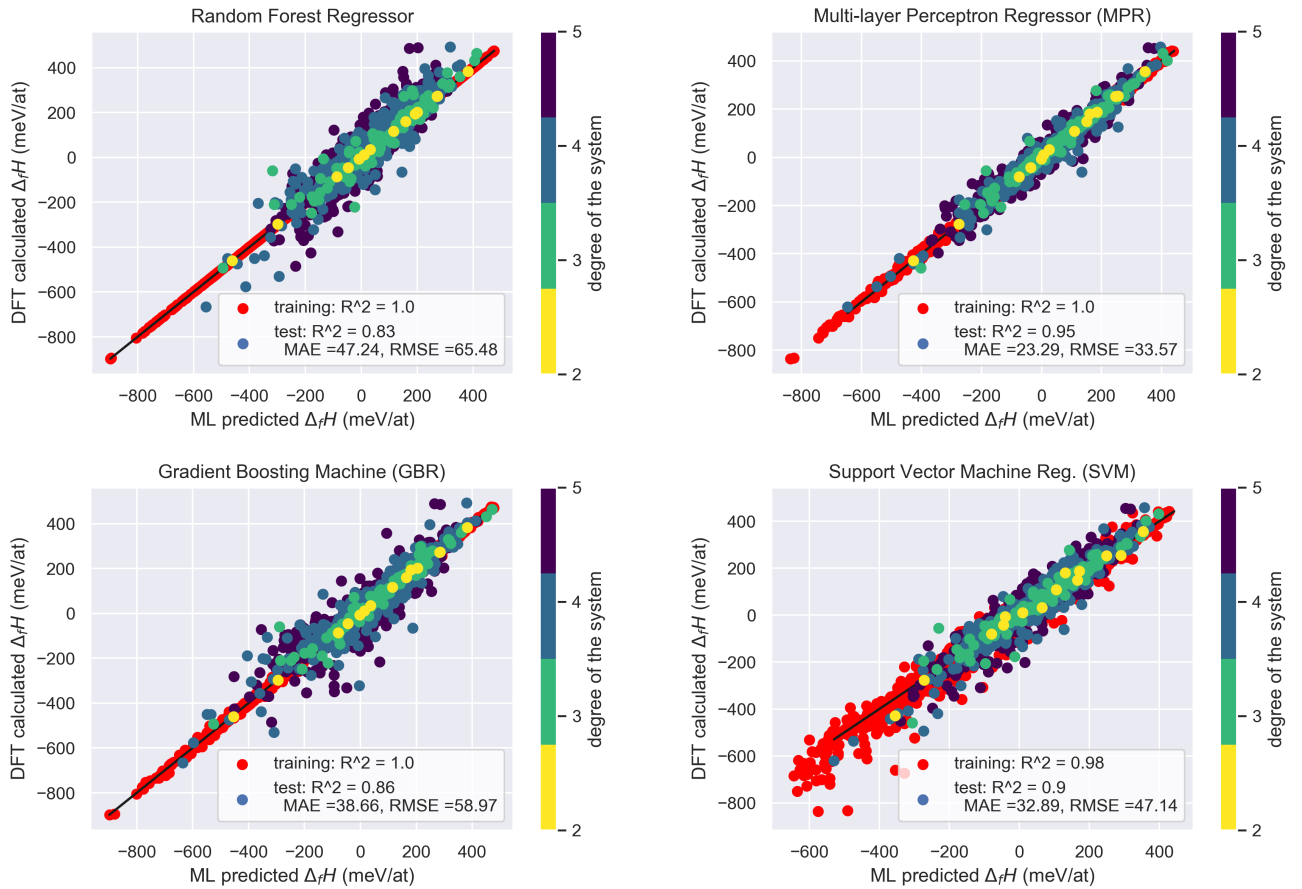


FIG. 2: Prediction of randomized 1001 configurations among the 537,824 ones from the learning of the training database (9974 data in red). The tested 1001 configurations are reported in colors (blue to yellow) corresponding to the degree d of their system (right side legend). The diagonal line indicates the perfect agreement between DFT calculated and ML predicted values.

III. DISCUSSION

A. Influence of the system degree

For the best method, here the regressor-type neural network MPR, the accuracy of prediction depends of the degree of the system of the tested configuration, illustrated by the color code of Fig. 2. As an example, the MAE \sim 23 meV for the whole testing set could be decomposed as contribution depending of the system degree d . It increases with d : 7 meV ($d = 2$), 22 ($d = 3$), 28 ($d = 4$) and 38 ($d = 5$). This result illustrates obviously that multi-component systems are more difficult to predict.

Another question could be addressed to the learning weight of binaries: does the whole $d = 1$ (14 elements) and $d = 2$ systems (here the 91 different sub-systems \times 30 configura-

tions) are sufficient to predict higher degree systems? In other words, is it possible to predict accurately the whole possible 14^5 combinations only from all unary and binary configurations (2744 unique data), which is representative of only 0.5% of the total set? In order to answer, we merged our training and testing sets leading to 10941 unique configurations and split them in the 5 sub-systems: 14 “ $d = 1$ ”, 2730 “ $d = 2$ ”, 5051 “ $d = 3$ ”, 2571 “ $d = 4$ ” and 575 “ $d = 5$ ” configurations. Then, from the all unique unary and binary configurations, we have tested the predictive behaviour for higher degree systems as shown in Fig. 3. Whereas the ternary and quaternary systems are well predicted with $\text{MAE} \sim 18$ and 22 meV respectively, the quinaries still present surprisingly reasonable results with $\text{MAE} \sim 34$ meV respectively. However, from higher to lower degree systems, a learning from a portion of the ternary configurations (5051 among the 54,600 possible) gives larger dispersion on prediction on the binaries with higher $\text{MAE} \sim 40$ meV and $\text{RMSE} \sim 73$ meV. Other combinations of training/testing subsystems are illustrated in SI-F.

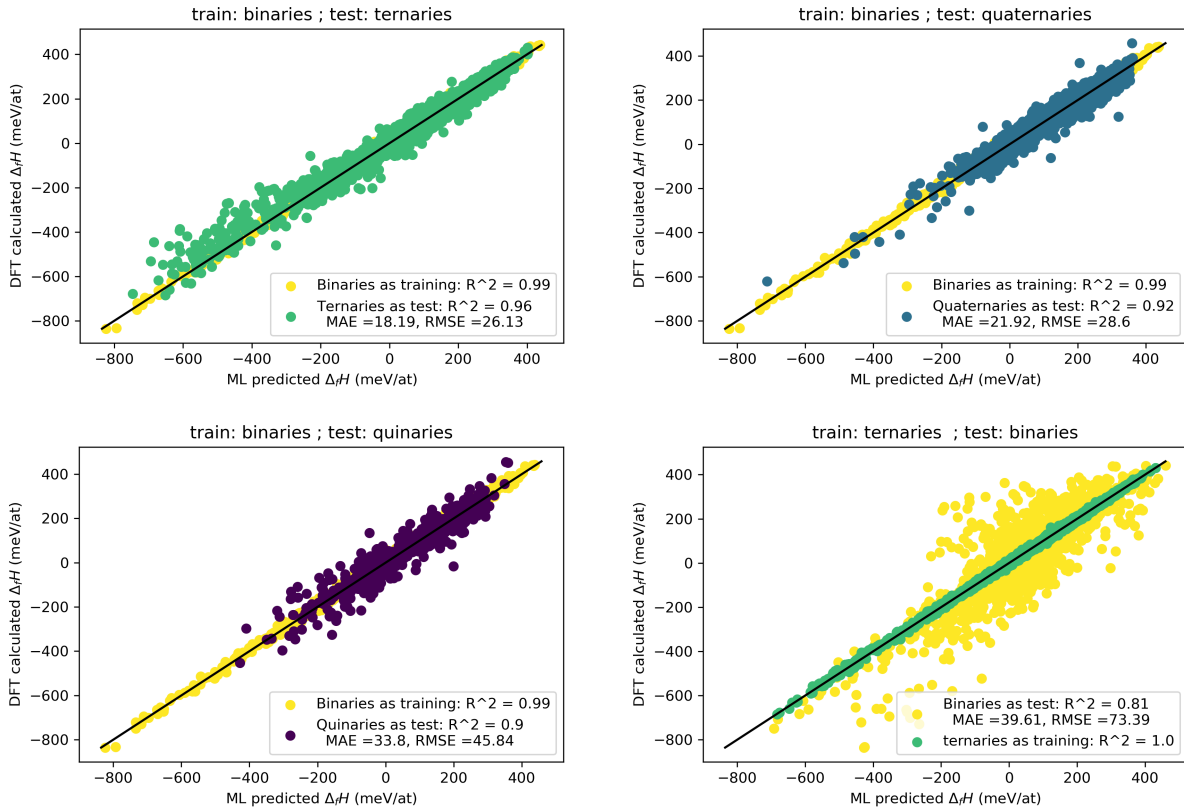


FIG. 3: From training on only binaries, prediction of ternaries, quaternaries or quinaries. The diagonal line indicates the perfect agreement between predicted and real values.

B. Contribution of additional descriptors

The consideration of additional physical descriptors improves slightly the learning scores. As shown in SI-G, the prediction with neither atomic radius nor the number of valence electron is slightly worse (MAE~24 with MPR). This result might seem unexpected at first glance. In fact, it is well known that topologically close packed (TCP) structures, as σ -phase, are driven by geometric arguments: since atoms are in the center of a coordination sphere, the atomic radius reflects the capability to occupy small or large coordination number (CN) sphere. The number of valence electron is also known to be important. In fact, for similar radius, a study has shown that the degeneracies of electronic levels plays a role on the site preference.³² To summarize this point, it looks that the total energy calculated by DFT contains these additional properties and does not need to be given in separated descriptors especially using a versatile deep learning approach like the MPR.

C. Prediction of crystal properties

The $\Delta_f H$ is only one predictive variable among many describing the crystal structure of the σ phase. Considering the only crystal definition, 9 variables are necessary to describe a configuration: 2 cell parameters (a, c) and 7 internal parameters ($x^{4f}, x^{8i_1}, y^{8i_1}, x^{8i_2}, y^{8i_2}, x^{8j}, z^{8j}$). In the present work, the supervised learning is optimized for predicting the $\Delta_f H$ but was also applied for every other variables and helps to initialize new DFT input files. In fact, it has been used to predict the starting structure of a large part of our learning database, and helped to reduce \sim 10 times the CPU consumption for the DFT relaxation steps. From our best model (optimized MPR) and from all available learning sets (9974+1001=10975 data), the predictive $\Delta_f H$ and the 9 other crystal variables are given for the every 537,824 configurations in SI-H. As an example, the prediction of both a & c tetragonal cell parameters presents a MAE~0.06 & 0.07 Å and a RMSE~0.08 & 0.10 respectively (SI-I).

D. Conclusions and outlook

This work addresses the issue of the crystal phase stability from the machine learning viewpoint. Because the $\Delta_f H$ is the key descriptor to model the formation of compounds, we have investigated the prediction of this variable using a supervised approach, using a complex crystallographic structure as an example: the σ -phase. Based on an unprecedented large first principles dataset containing about 10,000 compounds with $n = 14$ different elements, we optimized several supervised learning approaches, where the Multi-layers Perceptron Regressor presents best results to predict all the $\sim 500,000$ possible configurations within a mean absolute error of 23 meV ($\sim 2 \text{ kJ}\cdot\text{mol}^{-1}$). Additional descriptors with roots in the physical nature of the problem are minor contribution to the learning score in comparison with the only combinatorial DFT set. It is shown that the training database from the only binary-compositions (0.5% occurrence of whole set) are able to predict multicomponent configurations with a high accuracy. This result suggests that several complex phases including non-equivalent sites could be easily determined from the only binary contribution.

As an outlook, the learning database size will be increased up to twenty elements, including Ta and Si. This work will be extended to other complex TCP phases with more than 2 sites to demonstrate the efficiency of our approach, such as $A13$, $C14$, etc. Indeed, it opens broad avenues in the study of complex structures with the only binary configurations as a learning set, this could be efficient even with low number of data.

IV. METHODS

A. Training database from DFT calculations

First, a database from DFT calculations has been compiled. Since 2008, many active groups have calculated σ -phase configurations in binary^{32–36}, ternary^{37–40} and quaternary systems.⁴¹ Since all these sparse studies were calculated with different methods and parameters, our present original database includes only new calculations obtained under the same conditions, required millions of hours of CPU time to construct. The DFT methodology details are explained in SI-J. The learning database includes $n = 14$ different elements: Al, Co, Cr, Fe, Mn, Mo, Nb, Ni, Pt, Re, Ru, V, W, Zr, and contains 9974 unique configurations embracing all the $\binom{14}{2} = 91$ binaries (degree $d = 2$), 33 on the $\binom{14}{3} = 364$ ternaries ($d = 3$), 9 on the 1001 quaternaries ($d = 4$) and only 1 on the 2002 possible quinaries ($d = 5$, see SI-B for the combinatorial descriptions and SI-C for the detailed list of systems in our training database). The elemental distribution is not uniform because of some chemical reasons explaining that we wanted to have more data for pertinent systems (*e.g.* Zr-based σ -phase is not frequent). This analysis could be shown from SI-C 2. In addition, an independent testing set for 1001 randomized configuration were calculated (detailed in SI-E).

B. Database construction format

In a second step, data was arranged as a learning database, $X_{ijklm} \in \mathbb{R}^{(n+2)s \times N}$. The $n = 14$ elements are categorical variables but need to be treated with analytical methods that require numbers. Thus, each of the 5 crystal sites (i, j, k, l, m) has been considered as a 14-dim vector of dummies (spin variables: 0 or 1) by the one hot encoding method. In addition, because it is well known that the stability in this kind of compounds is driven by the two geometric and electronic constraints²⁷ (*e.g.* large electropositive atoms have a preference on high coordination sites), atom size and electron concentration have been used as additional descriptors. In total, we use a set of $p = (n+2)s = 80$ attributes corresponding to the following features for each configuration X_{ijklm} , with $(i, j, k, l, m) \in \{ \text{Al, Co, Cr, ..., V, W, Zr} \}$:

- Ordering configuration of atoms in the crystal (14×5 vectors of dummies)

- Atomic radius (5 normalized values, related to the 5 atoms in $ijklm$ configuration)
- Number of valence electrons (5 normalized values)

leading to a 9974×80 matrix as the learning database, associated to the target y_{ijklm} vector, here the heat of formation, $\Delta_f H(ijklm)$, but could be any crystallographic properties such as cell parameters.

At last, based on the ML best results, the learning on the whole database (9974 configurations) was done and a final prediction of 1001 random configurations among the 537,824 was estimated.

C. Estimation of the machine learning models

The machine learning models mentioned above are estimated using Scikit-Learn 0.23 library in Python 3.5. Each approach offers different advantages, such as speed or interpretability, but our main goal was the high accuracy. Figure 4 illustrates the relationship between the model’s simplicity (interpretability) and the generalising performance for the machine learning methods we considered. Note that this scheme (Figure 4) is approximate. What is true for our results is that the linear methods perform worse than the non-linear regressions. We also noticed that the grid search for an optimal Multi-Layer Perceptron architecture (number of hidden layers and units), as well as the number of trees and their maximal depth in the Random Forest and Gradient Boosting, is important, and the search for an optimal configuration can be computationally expensive.

For each method, the corresponding hyper-parameters were fixed using the grid search module and the cross-validation error rate. The generalising performance is the test accuracy using 10-fold cross validation procedure: the database is randomly split into 10 subsets (folds), and the model is trained on 9 parts, and tested on 1 part. The procedure is repeated 10 times. The average test accuracy is the mean value over performances on the test data.

Below, we provide a short description of the considered machine learning methods. The data consists in N observations $\{X_i, y_i\}_{i=1}^N$, where $y \in \mathbb{R}$. Each observation is a vector of length p , where p is the number of features (parameters), $p = 80$ in our case.

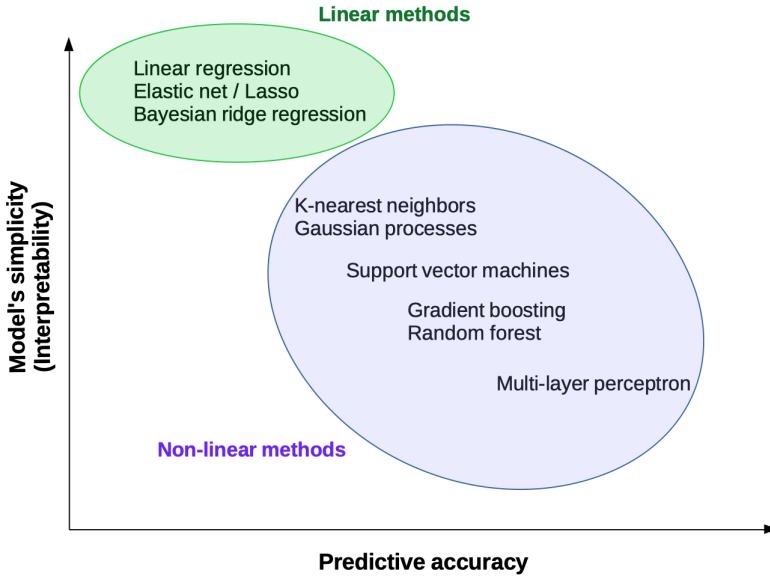


FIG. 4: A schematic representation of the models' simplicity and the generalising accuracy for the tested Machine Learning approaches.

- *Ordinary least squared linear regression.* The predicted value is modelled as follows:

$$y_i = \beta_1 x_{i1} + \beta_2 x_{i2} + \cdots + \beta_p x_{ip} + \epsilon_i, \quad (4)$$

where ϵ_i is unobserved noise. To avoid overfitting, the loss function is penalised by the L_2 penalty term, also known as Ridge regression:

$$\hat{\beta} = \arg \min_{\beta} \|y - X\beta\|_2^2 + \lambda \|\beta\|_2^2, \quad (5)$$

where λ is associated with the penalty term, and is usually fixed using the grid search.

- *Elastic net linear regression.* The elastic net is a combination of the L_1 and L_2 penalty terms:

$$\hat{\beta} = \arg \min_{\beta} \|y - X\beta\|_2^2 + \lambda_2 \|\beta\|_2^2 + \lambda_1 \|\beta\|_1. \quad (6)$$

In case where $\lambda_1 = 0$, we get the above mentioned ridge regression, and if $\lambda_2 = 0$, the problem boils down to the Lasso. An optimal choice of λ_1 and λ_2 leads to a sparse

but accurate model. The number of parameters is quite small in our database, and the feature selection is not relevant for our case.

- *Random forest regression (RFR)*. The random forest approach is an ensemble non-linear machine learning method that fits a number of decision trees (number of estimators) that vote for the final decision. A number of hyper-parameters, such as the number of trees and their maximal depth has to be fixed (usually via the cross validation) to achieve a reasonable trade off between the model’s complexity and the generalising performance.
- *Gradient boosting regression (GBR)*. The gradient boosting method constructs an additive model. At each iteration of the learning procedure, a new regression tree which corrects the current model, is added. Similarly to the random forest, here also, the number of trees (or the number of estimators) and their maximal depth are important hyper-parameters that control the model’s complexity and accuracy (very deep decision trees are likely to lead to overfitting).
- *Multi-layer Perceptron Regression (MPR)*. A multi-layer perceptron (or artificial neural network) includes an input layer, several (or at least one) hidden layers, and an output layer. In our experiments, we use three hidden layers, and we get the following transformations:

$$f(X) = h\left(b^3 + W^3 h\left(b^2 + W^2 h(b^1 + W^1 X)\right)\right), \quad (7)$$

where h is the activation function, and in our experiments tanh is chosen $h(a) = (e^a - e^{-a})/(e^a + e^{-a})$. The parameters to estimate are $\{b^1, W^1, b^2, W^2, b^3, W^3\}$. The optimised function is the squared loss function. We use a stochastic gradient descent.

- *Support vector regression (SVM)*. We use the ϵ -support vector regression with the rbf (radial basis function) kernel that leads to a non-linear separator. The loss function is penalised by the L_2 norm, and the hyper-parameter C which is the regularisation parameter, is to be fixed. The choice of the non-linear kernel is motivated by our results with both linear (linear regression) and non-linear (MPR, boosting, random forest) methods, illustrating that the non-linear approaches are more efficient for our

task.

- *K-nearest neighbours.* The algorithm uses similarity between points to predict the values of new instances. We use the Manhattan distance, since it is more robust against the outliers. First, the distance between a new point and all available data is computed. Then, the k nearest neighbours are selected, and the average of these points is the predicted value. For our experiments, we fixed $k = 3$.
- *Bayesian ridge regression.* The method is a ridge regression in the Bayesian viewpoint, and it uses probability distributions rather than point estimates. The response y is assumed to be drawn from a probability distribution

$$y = \mathcal{N}(\beta^T X, \sigma^2 I), \quad (8)$$

where σ is the standard deviation, $\mathcal{N}(\cdot)$ is a normal (Gaussian) distribution, T stands for *transpose*, and I is the identity. The goal of the Bayesian approach is rather to determine the posterior distribution for the parameters of the model:

$$\mathbb{P}(\beta|X, y) = \frac{\mathbb{P}(y|\beta, X)\mathbb{P}(\beta|X)}{\mathbb{P}(y|X)}. \quad (9)$$

- *Gaussian process regression (GPR).* The approach is non-parametric and Bayesian. A Gaussian process is like a multivariate Gaussian distribution in an infinite dimension, and any collection of labels of a data set are joint Gaussian distributed:

$$y \sim \text{GP}(m(X), k(X, X')), \quad (10)$$

where $m(\cdot)$ is a mean function, and $k(\cdot)$ is a covariance function.

Data and code availability

All data generated in this study are available from the authors on request, and will be included in the regular publication version.

Acknowledgements

We wish to acknowledge the support of the GENCI-CINES: DFT calculations were performed using their HPC resources (Grant A0060906175). In addition, we acknowledge the financial support from the CNRS (programs MaLeFHYCe, PEPS, Cellule Energie CNRS and MALEpHYq, Emergence@INC)

Author contributions

JCC designed the project, performed the calculation. JMJ analysed the results as Calphad output. NS performed the machine learning optimization. All the authors together finalized the manuscript.

Competing Interests

The authors declare no competing interests

Additional Information

Supplementary information is available for this paper in several Appendix.

References

- * Electronic address: crivello@icmpe.cnrs.fr
- ¹ S. H. Lee, “Natural language generation for electronic health records,” *npj Digital Medicine*, vol. 1, p. 63, Nov. 2018.
- ² M. H. S. Segler, T. Kogej, C. Tyrchan, and M. P. Waller, “Generating focused molecule libraries for drug discovery with recurrent neural networks,” *ACS Central Science*, vol. 4, no. 1, pp. 120–131, 2018. PMID: 29392184.
- ³ P. Ruamviboonsuk, J. Krause, P. Chotcomwongse, R. Sayres, R. Raman, K. Widner, B. J. L. Campana, S. Phene, K. Hemarat, M. Tadarati, S. Silpa-Archa, J. Limwattanayingyong, C. Rao,

- O. Kuruvilla, J. Jung, J. Tan, S. Orprayoon, C. Kangwanwongpaisan, R. Sukumalpaiboon, C. Luengchaichawang, J. Fuangkaew, P. Kongsap, L. Chualinpha, S. Saree, S. Kawinpanitan, K. Mitvongsa, S. Lawanasakol, C. Thepchatri, L. Wongpichedchai, G. S. Corrado, L. Peng, and D. R. Webster, “Deep learning versus human graders for classifying diabetic retinopathy severity in a nationwide screening program,” *npj Digital Medicine*, vol. 2, no. 1, pp. 25–, 2019.
- ⁴ J. Schmidt, M. R. G. Marques, S. Botti, and M. A. L. Marques, “Recent advances and applications of machine learning in solid-state materials science,” *npj Computational Materials*, vol. 5, no. 1, pp. 83–, 2019.
- ⁵ V. Tshitoyan, J. Dagdelen, L. Weston, A. Dunn, Z. Rong, O. Kononova, K. A. Persson, G. Ceder, and A. Jain, “Unsupervised word embeddings capture latent knowledge from materials science literature,” *Nature*, vol. 571, pp. 95–98, July 2019.
- ⁶ L. Ward, A. Agrawal, A. Choudhary, and C. Wolverton, “A general-purpose machine learning framework for predicting properties of inorganic materials,” *npj Computational Materials*, vol. 2, no. 1, pp. 16028–, 2016.
- ⁷ Z. Zhou, Y. Zhou, Q. He, Z. Ding, F. Li, and Y. Yang, “Machine learning guided appraisal and exploration of phase design for high entropy alloys,” *npj Computational Materials*, vol. 5, no. 1, pp. 128–, 2019.
- ⁸ T. Kostiuchenko, F. Körmann, J. Neugebauer, and A. Shapeev, “Impact of lattice relaxations on phase transitions in a high-entropy alloy studied by machine-learning potentials,” *npj Computational Materials*, vol. 5, no. 1, pp. 55–, 2019.
- ⁹ Z. Pei, J. Yin, J. A. Hawk, D. E. Alman, and M. C. Gao, “Machine-learning informed prediction of high-entropy solid solution formation: Beyond the hume-rothery rules,” *npj Computational Materials*, vol. 6, no. 1, pp. 50–, 2020.
- ¹⁰ J. Peng, Y. Yamamoto, J. A. Hawk, E. Lara-Curzio, and D. Shin, “Coupling physics in machine learning to predict properties of high-temperatures alloys,” *npj Computational Materials*, vol. 6, no. 1, pp. 141–, 2020.
- ¹¹ S. K. Kauwe, J. Graser, A. Vazquez, and T. D. Sparks, “Machine learning prediction of heat capacity for solid inorganics,” *Integrating Materials and Manufacturing Innovation*, vol. 7, no. 2, pp. 43–51, 2018.
- ¹² G. Pilania, A. Mannodi-Kanakkithodi, B. P. Uberuaga, R. Ramprasad, J. E. Gubernatis, and T. Lookman, “Machine learning bandgaps of double perovskites,” *Scientific Reports*, vol. 6,

- no. 1, pp. 19375–, 2016.
- ¹³ V. Gladkikh, D. Y. Kim, A. Hajibabaei, A. Jana, C. W. Myung, and K. S. Kim, “Machine learning for predicting the band gaps of abx₃ perovskites from elemental properties,” *The Journal of Physical Chemistry C*, vol. 124, no. 16, pp. 8905–8918, 2020.
- ¹⁴ B. Meredig, A. Agrawal, S. Kirklin, J. E. Saal, J. W. Doak, A. Thompson, K. Zhang, A. Choudhary, and C. Wolverton, “Combinatorial screening for new materials in unconstrained composition space with machine learning,” *Phys. Rev. B*, vol. 89, p. 094104, Mar 2014.
- ¹⁵ S. Kirklin, J. E. Saal, B. Meredig, A. Thompson, J. W. Doak, M. Aykol, S. Rühl, and C. Wolverton, “The open quantum materials database (oqmd): assessing the accuracy of dft formation energies,” *npj Computational Materials*, vol. 1, no. 1, p. 15010, 2015.
- ¹⁶ S. Ubaru, A. Międlar, Y. Saad, and J. R. Chelikowsky, “Formation enthalpies for transition metal alloys using machine learning,” *Phys. Rev. B*, vol. 95, p. 214102, Jun 2017.
- ¹⁷ C. J. Bartel, A. Trewartha, Q. Wang, A. Dunn, A. Jain, and G. Ceder, “A critical examination of compound stability predictions from machine-learned formation energies,” *npj Computational Materials*, vol. 6, no. 1, pp. 97–, 2020.
- ¹⁸ C. Osse, C. Toher, and S. Curtarolo, “Data-driven design of inorganic materials with the automatic flow framework for materials discovery,” *MRS Bulletin*, vol. 43, no. 9, p. 670–675, 2018.
- ¹⁹ C. Draxl and M. Scheffler, “Nomad: The fair concept for big data-driven materials science,” *MRS Bulletin*, vol. 43, no. 9, p. 676–682, 2018.
- ²⁰ A. M. Deml, R. O’Hayre, C. Wolverton, and V. Stevanović, “Predicting density functional theory total energies and enthalpies of formation of metal-nonmetal compounds by linear regression,” *Phys. Rev. B*, vol. 93, p. 085142, Feb 2016.
- ²¹ Y. Liu, T. Zhao, W. Ju, and S. Shi, “Materials discovery and design using machine learning,” *Journal of Materomics*, vol. 3, no. 3, pp. 159 – 177, 2017. High-throughput Experimental and Modeling Research toward Advanced Batteries.
- ²² Y. Kim, E. Kim, E. Antono, B. Meredig, and J. Ling, “Machine-learned metrics for predicting the likelihood of success in materials discovery,” *npj Computational Materials*, vol. 6, no. 1, pp. 131–, 2020.
- ²³ A. Jain, S. P. Ong, G. Hautier, W. Chen, W. D. Richards, S. Dacek, S. Cholia, D. Gunter, D. Skinner, G. Ceder, and K. A. Persson, “Commentary: The materials project: A materials

genome approach to accelerating materials innovation,” *APL Materials*, vol. 1, no. 1, p. 011002, 2013.

- ²⁴ A. Miedema, R. Boom, and F. De Boer, “On the heat of formation of solid alloys,” *J. Less-Common Met.*, vol. 41, pp. 283–298, July 1975.
- ²⁵ L. Kaufman and H. Bernstein, *Computer Calculation of Phase Diagrams with Special Reference to Refractory Metals*. Notes and Reports in Computer Science and Applied Mathematic, Academic Press, 1970.
- ²⁶ B. Sundman and J. Ågren, “A regular solution model for phases with several components and sublattices, suitable for computer applications,” *J. Phys. Chem. Solids*, vol. 42, pp. 297–301, 1981.
- ²⁷ J.-M. Joubert, “Crystal chemistry and calphad modeling of the σ phase,” *Prog. Mater. Sci.*, vol. 53, pp. 528–583, 2008.
- ²⁸ R. Mathieu, N. Dupin, J.-C. Crivello, K. Yaqoob, A. Breidi, J.-M. Fiorani, N. David, and J.-M. Joubert, “CALPHAD description of the Mo–Re system focused on the sigma phase modeling,” *Calphad*, vol. 43, no. 0, pp. 18–31, 2013.
- ²⁹ N. Dupin, U. Kattner, B. Sundman, M. Palumbo, and S. Fries, “Implementation of an effective bond energy formalism in the multicomponent calphad approach,” *J Res Natl Inst Stan*, vol. 123, p. 123020, 2018.
- ³⁰ D. Jha, L. Ward, A. Paul, W.-k. Liao, A. Choudhary, C. Wolverton, and A. Agrawal, “Elemnet: Deep learning the chemistry of materials from only elemental composition,” *Scientific Reports*, vol. 8, no. 1, pp. 17593–, 2018.
- ³¹ Z. Zhang, M. Li, K. Flores, and R. Mishra, “Machine learning formation enthalpies of intermetallics,” *Journal of Applied Physics*, vol. 128, no. 10, p. 105103, 2020.
- ³² M. H. F. Sluiter and A. Pasturel, “Site occupation in the Cr-Ru and Cr-Os σ phases,” *Phys. Rev. B*, vol. 80, p. 134122, Oct 2009.
- ³³ C. Berne, M. H. F. Sluiter, Y. Kawazoe, T. Hansen, and A. Pasturel, “Site occupancy in the Re-W sigma phase,” *Phys. Rev. B*, vol. 64, p. 144103, 2001.
- ³⁴ P. Korzhavyi, B. Sundman, M. Selleby, and B. Johansson, “Atomic, electronic, and magnetic structure of iron-based sigma-phases,” *Mater. Res. Soc. Symp. Proc.*, vol. 842, p. S4.10.1, 2005.
- ³⁵ J. Cieslak, J. Tobola, and S. M. Dubiel, “Electronic structure of the σ phase of paramagnetic Fe-V alloys,” *Phys. Rev. B*, vol. 81, p. 174203, May 2010.

- ³⁶ M. Palumbo, T. Abe, C. Kocer, H. Murakami, and H. Onodera, “Ab initio and thermodynamic study of the Cr-Re system,” *Calphad*, vol. 34, pp. 495–503, Dec. 2010.
- ³⁷ K. Chvátalová, J. Houšerová, M. Šob, and J. Vřeštál, “First-principles calculations of energetics of sigma phase formation and thermodynamic modelling in Fe-Ni-Cr system,” *J. Alloys Comp.*, vol. 378, pp. 71–74, Sept. 2004.
- ³⁸ J.-C. Crivello, M. Palumbo, T. Abe, and J.-M. Joubert, “*Ab initio* ternary σ -phase diagram: the Cr-Mo-Re system,” *Calphad*, vol. 34, pp. 487–494, 2010.
- ³⁹ M. Palumbo, T. Abe, S. G. Fries, and A. Pasturel, “First-principles approach to phase stability for a ternary sigma phase: Application to Cr-Ni-Re,” *Phys. Rev. B*, vol. 83, p. 144109, Apr. 2011.
- ⁴⁰ K. Yaqoob, J.-C. Crivello, and J.-M. Joubert, “Study of site occupancies in Mo-Ni-Re sigma-phase by both experimental and ab initio methods,” *Inorg. Chem.*, vol. 51, pp. 3071–3078, 2012.
- ⁴¹ J.-C. Crivello, R. Souques, A. Breidi, N. Bourgeois, and J.-M. Joubert, “Zengen, a tool to generate ordered configurations for systematic first-principles calculations: The cr-mo-ni-re system as a case study,” *Calphad*, vol. 51, pp. 233 – 240, 2015.
- ⁴² P. Hohenberg and W. Kohn, “Inhomogeneous electron gas,” *Phys. Rev.*, vol. 136, no. 3B, pp. B864–B871, 1964.
- ⁴³ W. Kohn and L. Sham, “Self-consistent equations including exchange and correlation effects,” *Phys. Rev.*, vol. 140, no. 4A, pp. A1133–1140, 1965.
- ⁴⁴ G. Kresse and J. Hafner, “Ab initio molecular dynamics for liquid metals,” *Phys. Rev. B*, vol. 47, no. 1, pp. 558–561, 1993.
- ⁴⁵ G. Kresse and J. Furthmüller, “Efficient iterative schemes for ab initio total-energy calculations using a plane-wave basis set,” *Phys. Rev. B*, vol. 54, pp. 11169–11186, Oct 1996.
- ⁴⁶ G. Kresse and D. Joubert, “From ultrasoft pseudopotentials to the projector augmented-wave method,” *Phys. Rev. B*, vol. 59, no. 3, pp. 1758–1775, 1999.
- ⁴⁷ P. E. Blöchl, “Projector augmented-wave method,” *Phys. Rev. B*, vol. 50, no. 24, pp. 17953–17979, 1994.
- ⁴⁸ J. P. Perdew, K. Burke, and M. Ernzerhof, “Generalized gradient approximation made simple,” *Phys. Rev. Lett.*, vol. 77, pp. 3865–3868, 1996.
- ⁴⁹ J. P. Perdew, K. Burke, and M. Ernzerhof, “Erratum: Generalized gradient approximation

- made simple,” *Phys. Rev. Lett.*, vol. 78, no. 7, p. 1396, 1997.
- ⁵⁰ H. Monkhorst and J. Pack, “Special points for Brillouin-zone integrations,” *Phys. Rev. B*, vol. 13, pp. 5188–5192, 1976.
- ⁵¹ P. E. Blöchl, O. Jepsen, and O. K. Andersen, “Improved tetrahedron method for Brillouin-zone integrations,” *Phys. Rev. B*, vol. 49, no. 23, p. 16223, 1994.
- ⁵² K. Momma and F. Izumi, “VESTA3 for three-dimensional visualization of crystal, volumetric and morphology data,” *J. Appl. Crystallogr.*, vol. 44, pp. 1272–1276, Dec 2011.
- ⁵³ L. Chaput, A. Togo, I. Tanaka, and G. Hug, “Phonon-phonon interactions in transition metals,” *Phys. Rev. B*, vol. 84, p. 094302, 2011.

Appendix A: Crystal details of the σ -phase

The crystal structure of the σ -phase is tetragonal, described by the $P4_2/mnm$ space group (no. 136), with five non-equivalent positions ($s = 5$). Depending on the system, the cell parameters a and c take experimental values from 8.78 to 10.06 Å and 4.55 to 5.23 Å respectively. The σ -phase belongs to the Frank–Kasper or topologically close packed phases, characterized by the unique presence of tetrahedral interstices, and a limited number of coordination polyhedra.²⁷

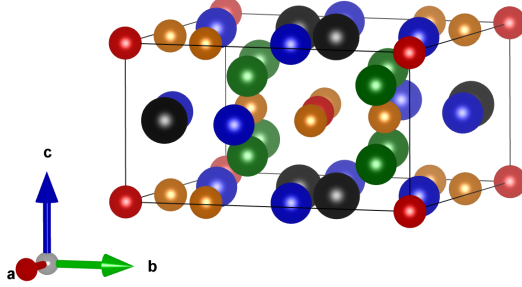


FIG. 5: Representation of the primitive cell of the crystal phase σ -phase ($D8_b$), with its 5 non-equivalent sites: 2a (red balls), 4f (black), 8i₁ (blue), 8i₁ (orange) and 8j (green).

TABLE II: Crystal structure of the σ -phase ($D8_b$): sites, Wyckoff positions, atomic positions (average values) in the $P4_2/mnm$ space group (no. 136). Details of the first neighbors number and their ratio, and coordination number (CN).

Site	Wyc.	x	y	z	i	j	k	l	m	ratio	CN
i	2a	0	0	0	0	4	0	4	4	0	12
j	4f	$\simeq 0.399$	x	0	2	1	2	4	6	0.07	15
k	8i ₁	$\simeq 0.464$	$\simeq 0.131$	0	0	1	5	4	4	0.36	14
l	8i ₂	$\simeq 0.741$	$\simeq 0.066$	0	1	2	4	1	4	0.08	12
m	8j	$\simeq 0.187$	x	$\simeq 0.251$	1	3	4	4	2	0.14	14

Appendix B: Analysis of the combinatorial descriptions

Considering a set of $n = 14$ different elements that could be arranged in a crystallographic phase φ of $s = 5$ inequivalent sites, there is a total of $N = 14^5 = 537,824$ unique configurations. The system of n elements is composed of sub-systems of degree $d \leq s$ that could describe a unique φ configuration. Each subsystem owns d^5 configurations, that could be decomposed in a number of sub-systems of lower degree as detailed in Table bellow. In addition, the numbers of subsystems is given by a binomial coefficient $\binom{n}{d} = \frac{n!}{d!(n-d)!}$, e.g. there is $\binom{14}{4} = 1001$ quaternary systems for $n = 14$. A summary of the combinatorial descriptions is given in the following Table and figure.

TABLE III: For a system with $n = 14$ elements distributed in a phase φ of $s = 5$ sites, are given: degree d of a subsystem, number of configuration d^5 , number of configuration in each subsystem of lower degree $d \leq s$, number of different subsystems, total and proportion of the number of configurations.

d	d^5	$N(d = 1)$	$N(d = 2)$	$N(d = 3)$	$N(d = 4)$	$N(d = 5)$	$\binom{n}{d}$	N
1	1	1	0	0	0	0	14	14 (0.0%)
2	32	2	30	0	0	0	91	2,730 (0.51%)
3	243	3	3×30	150	0	0	364	54,600 (10.15%)
4	1024	4	6×30	4×150	240	0	1,001	240,240 (44.67%)
5	3125	5	10×30	10×150	5×240	120	1,001	240,240 (44.67%)

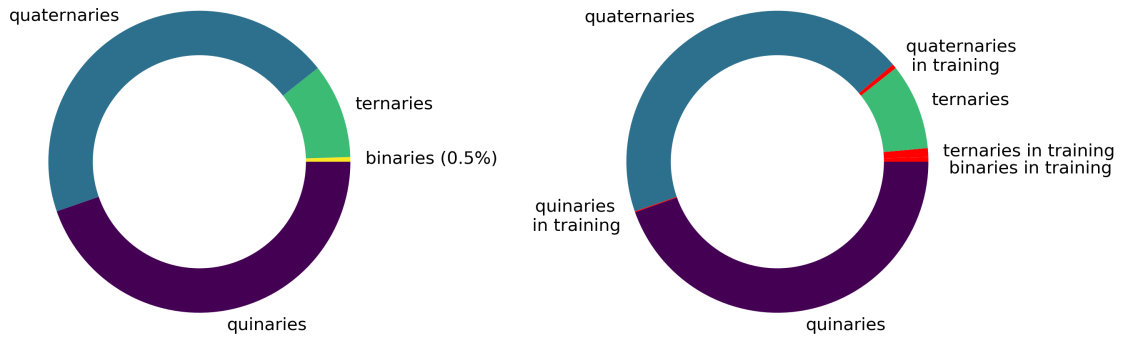


FIG. 6: Proportion of sub-systems in the whole set for $s = 5$ and $n = 14$ (537,824 unique configurations) (left) and calculated sub-systems included in the learning database in red (right).

Appendix C: The training database, 9974 configurations

1. List of systems included in the training database

91 binary systems with all the corresponding $2^5 = 32$ configurations, 91 among $\binom{14}{2} = 91$:

[’Al’, ’Co’], [’Al’, ’Cr’], [’Co’, ’Cr’], [’Al’, ’Fe’], [’Co’, ’Fe’],
[’Cr’, ’Fe’], [’Al’, ’Mn’], [’Co’, ’Mn’], [’Cr’, ’Mn’], [’Fe’, ’Mn’],
[’Al’, ’Mo’], [’Co’, ’Mo’], [’Cr’, ’Mo’], [’Fe’, ’Mo’], [’Mn’, ’Mo’],
[’Al’, ’Nb’], [’Co’, ’Nb’], [’Cr’, ’Nb’], [’Fe’, ’Nb’], [’Mn’, ’Nb’],
[’Mo’, ’Nb’], [’Al’, ’Ni’], [’Co’, ’Ni’], [’Cr’, ’Ni’], [’Fe’, ’Ni’],
[’Mn’, ’Ni’], [’Mo’, ’Ni’], [’Nb’, ’Ni’], [’Al’, ’Pt’], [’Co’, ’Pt’],
[’Cr’, ’Pt’], [’Fe’, ’Pt’], [’Mn’, ’Pt’], [’Mo’, ’Pt’], [’Nb’, ’Pt’],
[’Ni’, ’Pt’], [’Al’, ’Re’], [’Co’, ’Re’], [’Cr’, ’Re’], [’Fe’, ’Re’],
[’Mn’, ’Re’], [’Mo’, ’Re’], [’Nb’, ’Re’], [’Ni’, ’Re’], [’Pt’, ’Re’],
[’Al’, ’Ru’], [’Co’, ’Ru’], [’Cr’, ’Ru’], [’Fe’, ’Ru’], [’Mn’, ’Ru’],
[’Mo’, ’Ru’], [’Nb’, ’Ru’], [’Ni’, ’Ru’], [’Pt’, ’Ru’], [’Re’, ’Ru’],
[’Al’, ’V’], [’Co’, ’V’], [’Cr’, ’V’], [’Fe’, ’V’], [’Mn’, ’V’],
[’Mo’, ’V’], [’Nb’, ’V’], [’Ni’, ’V’], [’Pt’, ’V’], [’Re’, ’V’],
[’Ru’, ’V’], [’Al’, ’W’], [’Co’, ’W’], [’Cr’, ’W’], [’Fe’, ’W’],
[’Mn’, ’W’], [’Mo’, ’W’], [’Nb’, ’W’], [’Ni’, ’W’], [’Pt’, ’W’],
[’Re’, ’W’], [’Ru’, ’W’], [’V’, ’W’], [’Al’, ’Zr’], [’Co’, ’Zr’],
[’Cr’, ’Zr’], [’Fe’, ’Zr’], [’Mn’, ’Zr’], [’Mo’, ’Zr’], [’Nb’, ’Zr’],
[’Ni’, ’Zr’], [’Pt’, ’Zr’], [’Re’, ’Zr’], [’Ru’, ’Zr’], [’V’, ’Zr’],
[’W’, ’Zr’].

33 ternary systems with all the corresponding $3^5 = 243$ configurations, 33 among $\binom{14}{3} = 364$:

[’Cr’, ’Fe’, ’Mn’], [’Cr’, ’Fe’, ’Mo’], [’Co’, ’Fe’, ’Ni’], [’Cr’, ’Fe’, ’Ni’],
[’Cr’, ’Mn’, ’Ni’], [’Fe’, ’Mn’, ’Ni’], [’Cr’, ’Mo’, ’Ni’], [’Al’, ’Nb’, ’Ni’],
[’Al’, ’Nb’, ’Pt’], [’Co’, ’Cr’, ’Re’], [’Cr’, ’Mo’, ’Re’], [’Mo’, ’Nb’, ’Re’],
[’Cr’, ’Ni’, ’Re’], [’Mo’, ’Ni’, ’Re’], [’Mo’, ’Pt’, ’Ru’], [’Al’, ’Fe’, ’V’],

[’Co’, ’Fe’, ’V’], [’Cr’, ’Fe’, ’V’], [’Cr’, ’Mn’, ’V’], [’Cr’, ’Mo’, ’V’],
 [’Fe’, ’Mo’, ’V’], [’Co’, ’Ni’, ’V’], [’Fe’, ’Ni’, ’V’], [’Cr’, ’Fe’, ’W’],
 [’Cr’, ’Mn’, ’W’], [’Fe’, ’Mn’, ’W’], [’Cr’, ’Ni’, ’W’], [’Fe’, ’Ni’, ’W’],
 [’Mn’, ’Ni’, ’W’], [’Mo’, ’Pt’, ’W’], [’Mo’, ’Ru’, ’W’], [’Pt’, ’Ru’, ’W’],
 [’Re’, ’W’, ’Zr’].

9 quaternary systems with all the corresponding $4^5 = 1024$ configurations, 9 among $\binom{14}{4} = 1001$:

[’Cr’, ’Fe’, ’Mn’, ’Ni’],
 [’Cr’, ’Mo’, ’Ni’, ’Re’],
 [’Cr’, ’Fe’, ’Mo’, ’V’],
 [’Co’, ’Fe’, ’Ni’, ’V’],
 [’Cr’, ’Fe’, ’Mn’, ’W’],
 [’Cr’, ’Fe’, ’Ni’, ’W’],
 [’Cr’, ’Mn’, ’Ni’, ’W’],
 [’Fe’, ’Mn’, ’Ni’, ’W’],
 [’Mo’, ’Pt’, ’Ru’, ’W’].

1 quinary system with all the corresponding $5^5 = 3125$ configurations, 1 among $\binom{14}{5} = 2002$:

[’Cr’, ’Fe’, ’Mn’, ’Ni’, ’W’].

2. Statistical analysis of the training database

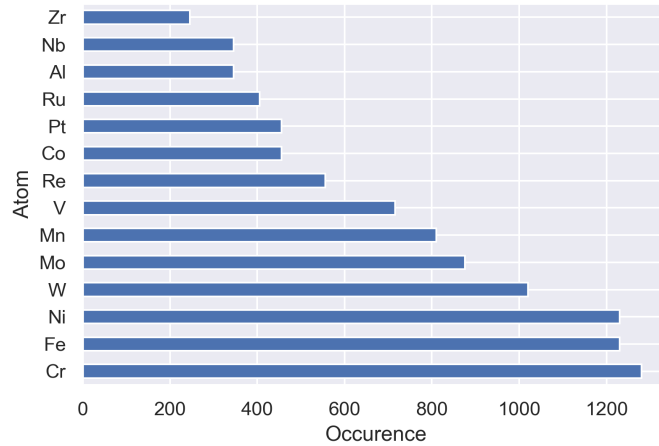


FIG. 7: Occurrence of the $n = 14$ elements in the training database (9974 entries).

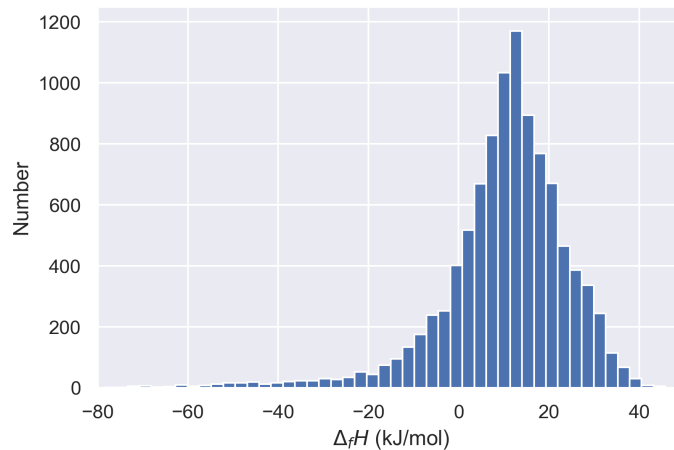


FIG. 8: Distribution of the heat of formation of the 9974 entries of the training database.

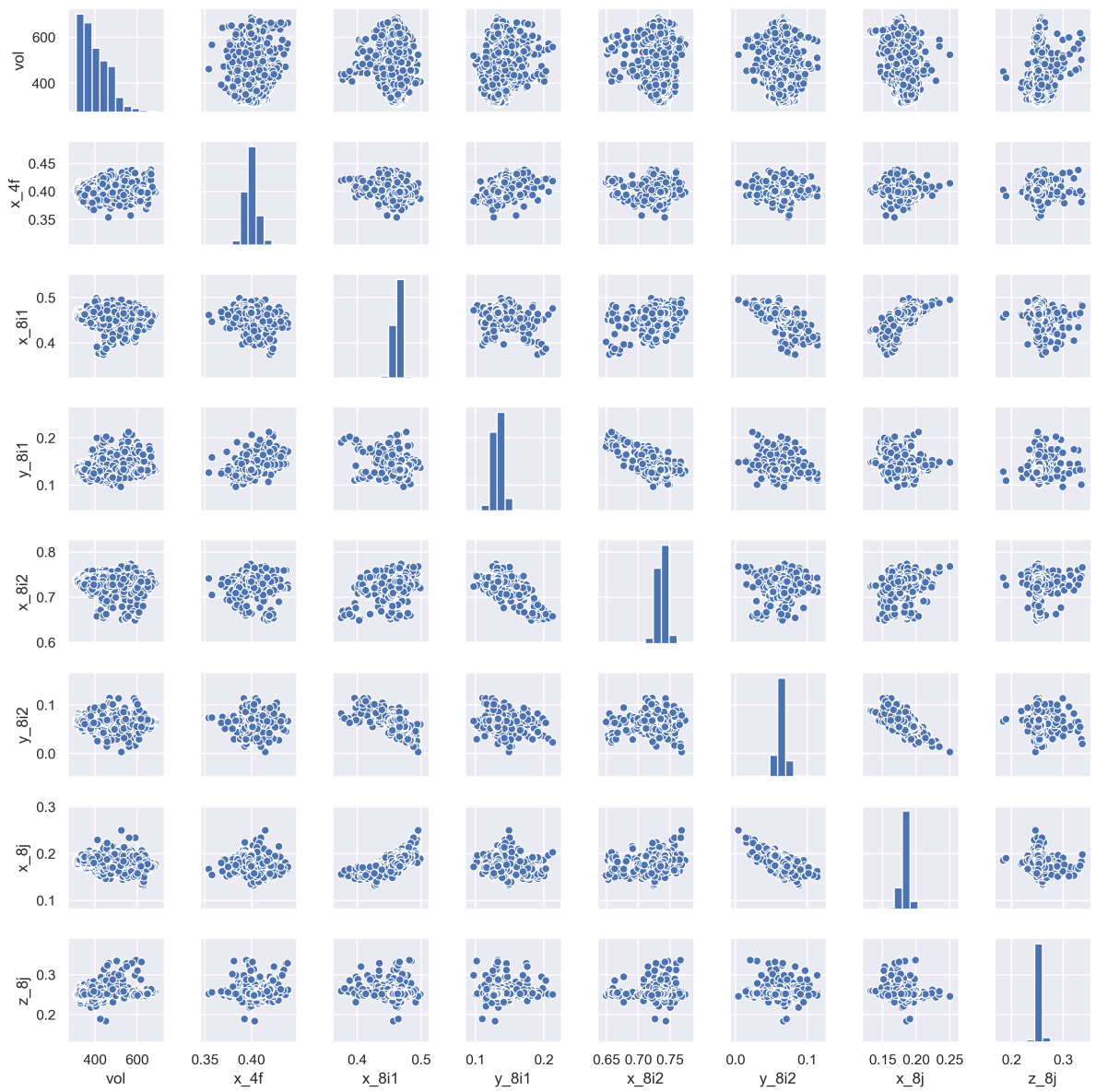


FIG. 9: Correlation matrix figures of cell parameters and internal positions of compounds in the training database.

Appendix D: Cross validation results from the only training database

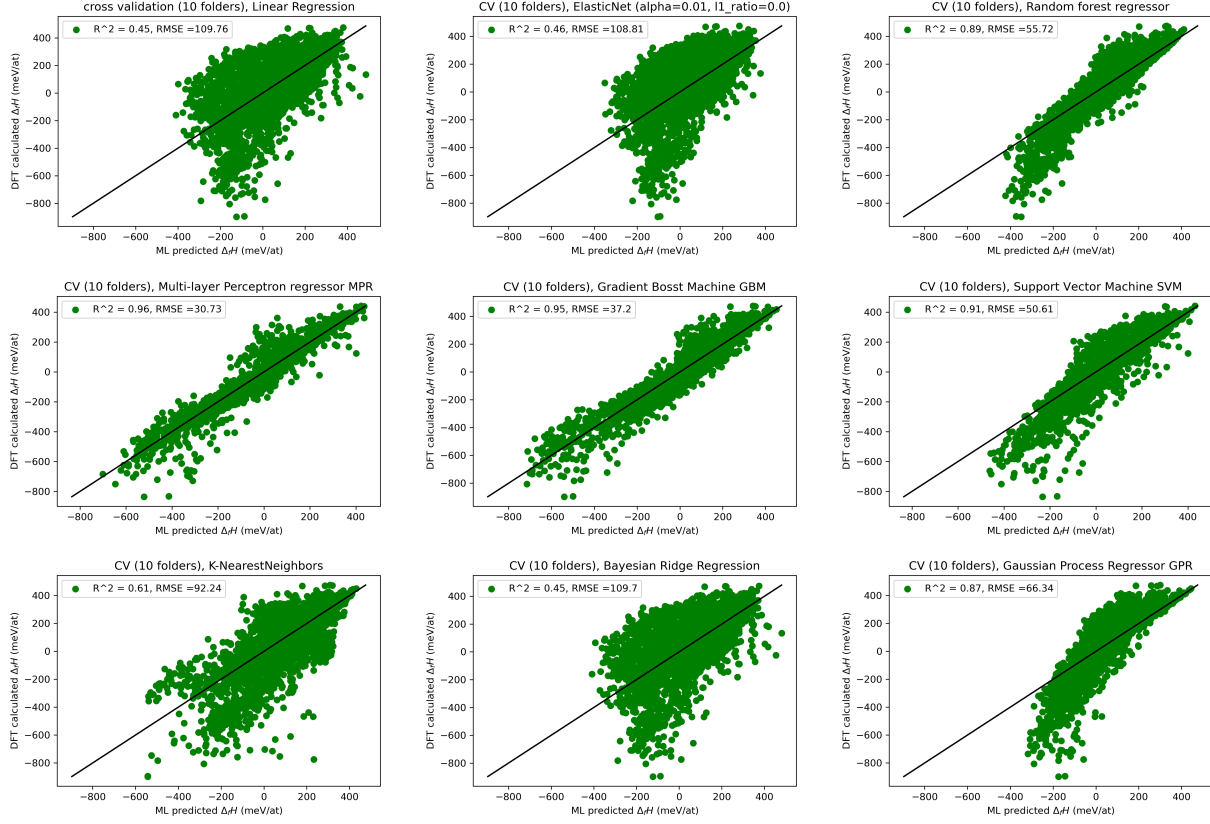


FIG. 10: Averaged results of prediction from various learning methods of $\sim 10,000$ compounds from cross validation under 10-folders. The diagonal line indicates the perfect agreement between DFT calculated and predicted values.

Appendix E: List of the 1001 testing set configurations

'Al:Co:Al:Co:Al', 'Al:Mo:Al:Mo:Al', 'Al:Mo:Mn:Re:Al', 'Al:Mo:Pt:Ru:Al', 'Al:Nb:Ni:Re:Re',
 'Al:Ni:Co:Mo:Ru', 'Al:Re:Fe:Al:Re', 'Co:Cr:V:Re:Co', 'Co:Fe:Cr:Co:Fe', 'Co:Fe:Ni:V:Mo',
 'Co:Fe:Ni:V:Ru', 'Co:Pt:Zr:Mo:Re', 'Co:Re:Re:V:Co', 'Cr:Cr:Cr:Nb:Zr', 'Cr:Fe:Mo:V:Mn',
 'Cr:Fe:Re:Re:Fe', 'Cr:Mn:Ni:W:Nb', 'Cr:Mn:Re:Re:Mn', 'Cr:Mo:Ni:Re:V', 'Cr:Mo:Re:Ni:V',
 'Cr:Pt:Al:Ni:Re', 'Cr:Re:Mn:Re:Pt', 'Cr:W:Cr:Mn:Pt', 'Cr:W:Mo:Cr:W', 'Cr:W:Mo:Ni:Cr',
 'Fe:Al:Re:Fe:Al', 'Fe:Cr:Co:Fe:Cr', 'Fe:Fe:Re:Mo:Re', 'Fe:Mn:Ni:W:Zr', 'Fe:Nb:Fe:Nb:Fe',
 'Fe:Re:Cr:Cr:Re', 'Fe:Re:Mn:Mn:Re', 'Fe:Re:V:Fe:Re', 'Fe:W:Fe:Zr:Mo', 'Mn:Mo:Re:Mn:Mo',
 'Mn:Ni:W:V:V', 'Mn:Re:Cr:Mn:Re', 'Mn:Re:V:Mn:Re', 'Mn:W:Cr:Ni:Fe', 'Mo:Co:Mo:Co:Mo',
 'Mo:Cr:W:Mo:Cr', 'Mo:Mn:Mo:Re:Re', 'Mo:Nb:Mn:V:Mn', 'Mo:Nb:Re:W:W', 'Mo:Pt:Ru:Al:Mo',
 'Mo:Pt:Ru:W:Re', 'Mo:V:Mn:Cr:Fe', 'Nb:Zr:Ru:Al:Mo', 'Ni:Al:Ni:Al:Ni', 'Ni:Mo:Nb:Re:W',
 'Ni:Nb:Cr:Mn:W', 'Ni:Zr:Fe:Mn:Ni', 'Pt:Re:Fe:Zr:Nb', 'Re:Al:Re:Al:Re', 'Re:Cr:Al:W:Al',
 'Re:Mo:Mo:Re:Fe', 'Re:Pt:Re:Pt:Re', 'Re:V:Co:Re:V', 'Re:V:Mn:Re:Mn', 'Ru:Co:Fe:Ni:V',
 'Ru:Co:Zr:Al:Nb', 'Ru:Pt:Re:Ru:Pt', 'V:Al:Ni:V:Mo', 'V:Fe:Fe:Re:V', 'V:Re:Cr:Co:V',
 'V:V:Cr:W:Re', 'V:Zr:W:Ni:Mo', 'W:Co:Co:W:Co', 'W:Cr:Ni:Mo:W', 'Zr:Ru:Mo:Co:Mo',
 'Al:Al:Co:Ni:Nb', 'Al:Al:Fe:Pt:Mo', 'Al:Al:Mn:Ni:Ru', 'Al:Al:Mn:Re:Co', 'Al:Al:Mo:V:Ni',
 'Al:Al:V:Ru:Mo', 'Al:Co:Cr:Mo:Zr', 'Al:Co:Cr:Ni:Ru', 'Al:Co:Re:Ru:Pt', 'Al:Co:V:Co:Re',
 'Al:Co:V:Nb:W', 'Al:Cr:Nb:Nb:Mn', 'Al:Cr:Ni:Mo:Ru', 'Al:Cr:Pt:Nb:Zr', 'Al:Cr:W:Co:Pt',
 'Al:Cr:W:Co:V', 'Al:Cr:Zr:Ru:Pt', 'Al:Fe:Al:Re:Ni', 'Al:Fe:Cr:Al:Ru', 'Al:Fe:Cr:Re:Pt',
 'Al:Fe:Fe:W:V', 'Al:Fe:Mn:Mo:Pt', 'Al:Fe:Mn:Mo:Re', 'Al:Fe:Mn:Re:Ru', 'Al:Fe:Re:Co:V',
 'Al:Fe:Ru:Al:Re', 'Al:Fe:Ru:Mo:Mo', 'Al:Fe:Zr:Al:Zr', 'Al:Mn:Cr:Fe:Fe', 'Al:Mn:Fe:Ni:Zr',
 'Al:Mn:Mo:Re:Ru', 'Al:Mn:Nb:Zr:Co', 'Al:Mn:Ru:Ni:V', 'Al:Mo:Co:Co:V', 'Al:Mo:Fe:V:Re',
 'Al:Mo:Ni:Mo:W', 'Al:Mo:Ni:Zr:W', 'Al:Mo:Zr:W:Mo', 'Al:Nb:Co:Mn:Zr', 'Al:Nb:Cr:Nb:Zr',
 'Al:Nb:Cr:W:Mo', 'Al:Nb:Fe:Al:Al', 'Al:Nb:Nb:Ni:Nb', 'Al:Nb:Ni:Zr:Re', 'Al:Nb:Pt:Zr:Fe',
 'Al:Nb:Ru:Re:Ni', 'Al:Nb:Ru:Zr:V', 'Al:Nb:Zr:Zr:V', 'Al:Ni:Mn:Cr:Al', 'Al:Ni:Mo:Re:Pt',
 'Al:Ni:Nb:Pt:Ru', 'Al:Ni:Ni:Co:Ni', 'Al:Ni:Re:Cr:Nb', 'Al:Ni:Ru:Nb:V', 'Al:Ni:W:Pt:Co',
 'Al:Pt:Al:V:Mn', 'Al:Pt:Mn:V:Mn', 'Al:Pt:V:Al:Ru', 'Al:Re:Cr:W:W', 'Al:Re:Re:Cr:Ru',
 'Al:Re:Ru:Ru:Ni', 'Al:Re:Ru:V:Cr', 'Al:Re:W:Pt:Cr', 'Al:Ru:Fe:Fe:Co', 'Al:Ru:Mn:Mo:Zr',
 'Al:Ru:Re:Re:Nb', 'Al:Ru:Ru:W:Cr', 'Al:Ru:V:Al:Fe', 'Al:Ru:V:Co:Mo', 'Al:Ru:V:Re:Nb',
 'Al:Ru:Zr:Mn:Nb', 'Al:V:Fe:W:Cr', 'Al:V:Mo:Mn:Mn', 'Al:V:Ni:V:Nb', 'Al:V:Pt:Re:Fe',
 'Al:W:Mo:Mo:Re', 'Al:W:Pt:Al:W', 'Al:W:Pt:Ni:Pt', 'Al:W:V:Fe:Mo', 'Al:Zr:Re:Pt:Cr',
 'Al:Zr:W:Co:Mo', 'Co:Al:Mo:Zr:Al', 'Co:Al:Nb:Mn:Pt', 'Co:Al:Pt:Re:Cr', 'Co:Al:Re:Re:Al',
 'Co:Al:Zr:V:Fe', 'Co:Co:Al:Zr:Cr', 'Co:Co:Cr:V:Mo', 'Co:Co:V:Co:Pt', 'Co:Cr:Al:Mo:Fe',
 'Co:Cr:Al:Nb:Cr', 'Co:Cr:Al:Zr:Ni', 'Co:Cr:Cr:Nb:Zr', 'Co:Cr:Nb:Re:V', 'Co:Cr:V:Ni:V',
 'Co:Cr:W:Mo:Re', 'Co:Cr:Zr:Cr:Re', 'Co:Cr:Zr:Fe:Al', 'Co:Fe:Fe:Mo:Ru', 'Co:Fe:Fe:W:Ni',
 'Co:Fe:Mo:Fe:Mo', 'Co:Fe:Re:Zr:Fe', 'Co:Fe:V:W:Ni', 'Co:Mn:Fe:Ru:Zr', 'Co:Mn:Ru:Mo:Ru',
 'Co:Mn:V:Mo:Mn', 'Co:Mo:Ni:Cr:Cr', 'Co:Mo:V:Re:Al', 'Co:Mo:W:Zr:Cr', 'Co:Mo:Zr:Nb:Ni',
 'Co:Nb:Al:Ru:Re', 'Co:Nb:Ni:Zr:Nb', 'Co:Nb:Ru:Pt:Mo', 'Co:Ni:Co:Mn:Al', 'Co:Ni:Mn:Al:V',
 'Co:Ni:Mo:Co:Re', 'Co:Ni:Ni:Mo:Pt', 'Co:Ni:Pt:Al:Ru', 'Co:Ni:Pt:Zr:Mn', 'Co:Ni:Re:Co:Re',
 'Co:Pt:Al:Pt:Pt', 'Co:Pt:Al:Ru:Fe', 'Co:Pt:Nb:Mn:Al', 'Co:Pt:Ni:Ni:Nb', 'Co:Pt:Pt:Nb:Cr',
 'Co:Pt:Ru:W:Zr', 'Co:Pt:V:Ni:Fe', 'Co:Re:Al:Mo:Cr', 'Co:Re:Co:Mo:Al', 'Co:Re:Nb:Zr:Al',
 'Co:Re:Zr:V:Co', 'Co:Ru:Cr:V:Mo', 'Co:Ru:Mn:Pt:V', 'Co:Ru:Ni:Ni:Zr', 'Co:Ru:Pt:Al:Al',
 'Co:V:Al:Fe:Mo', 'Co:V:Co:Mo:Mo', 'Co:V:Mo:Zr:Co', 'Co:V:Ni:Re:Zr', 'Co:V:Pt:W:Zr',
 'Co:V:W:Nb:W', 'Co:V:Zr:Fe:Ru', 'Co:W:Mo:Ru:Ni', 'Co:W:Re:Pt:Al', 'Co:W:Ru:Fe:W',
 'Co:W:W:Zr:Al', 'Co:Zr:Co:Ru:Mo', 'Co:Zr:Nb:Al:Al', 'Co:Zr:V:Mo:V', 'Cr:Al:Ni:Cr:Re',

'Cr:Al:Pt:Al:V', 'Cr:Al:Pt:Ni:Ru', 'Cr:Al:Zr:Nb:W', 'Cr:Co:Co:Mn:Ni', 'Cr:Co:Cr:Ni:Pt',
 'Cr:Co:Fe:Co:Ru', 'Cr:Co:Re:Mn:Pt', 'Cr:Co:Re:Ru:Al', 'Cr:Co:W:Zr:V', 'Cr:Co:Zr:Pt:Fe',
 'Cr:Cr:Cr:Nb:Zr', 'Cr:Cr:Re:Mo:Nb', 'Cr:Cr:V:Ru:Mn', 'Cr:Fe:Al:Co:Fe', 'Cr:Fe:Al:Cr:Pt',
 'Cr:Fe:Cr:Mn:Al', 'Cr:Fe:Ni:Al:Co', 'Cr:Fe:Ni:Mn:Al', 'Cr:Fe:Ru:Re:W', 'Cr:Fe:Ru:Ru:Nb',
 'Cr:Mn:Co:W:Pt', 'Cr:Mn:Fe:Re:Nb', 'Cr:Mn:Mo:W:Pt', 'Cr:Mo:Cr:Nb:Co', 'Cr:Mo:Fe:V:Zr',
 'Cr:Mo:Mn:Co:Cr', 'Cr:Mo:Pt:V:W', 'Cr:Mo:V:W:Co', 'Cr:Mo:W:Zr:Al', 'Cr:Nb:Fe:Cr:W',
 'Cr:Nb:Mo:Mn:V', 'Cr:Nb:Pt:Nb:Mo', 'Cr:Nb:V:Al:Fe', 'Cr:Nb:W:V:Al', 'Cr:Ni:Co:V:Co',
 'Cr:Ni:Nb:Mo:Ni', 'Cr:Ni:Pt:Zr:Mo', 'Cr:Ni:V:Ni:Ru', 'Cr:Pt:Co:Cr:Ru', 'Cr:Pt:Fe:Mo:Zr',
 'Cr:Pt:Mo:Ru:Zr', 'Cr:Pt:Ni:Mn:V', 'Cr:Pt:Ni:V:V', 'Cr:Pt:Pt:Mo:Re', 'Cr:Re:Co:Cr:Re',
 'Cr:Re:Fe:Al:Ru', 'Cr:Re:Mn:Re:Pt', 'Cr:Re:Ni:Re:Mo', 'Cr:Ru:Co:Re:Ru', 'Cr:Ru:Cr:Mo:Ru',
 'Cr:Ru:Cr:Nb:Re', 'Cr:Ru:Ni:Co:Mn', 'Cr:Ru:Ni:Re:Fe', 'Cr:V:Mo:Al:Ni', 'Cr:V:Nb:V:Zr',
 'Cr:V:Ni:W:Fe', 'Cr:V:Ru:Nb:W', 'Cr:V:Zr:Ni:Pt', 'Cr:W:Nb:Mn:Ni', 'Cr:W:Pt:Pt:Fe',
 'Cr:W:V:Zr:Ni', 'Cr:Zr:Ni:Cr:Ru', 'Cr:Zr:Ru:V:Co', 'Fe:Al:Al:W:W', 'Fe:Al:Co:Ni:Al',
 'Fe:Al:Cr:Mo:Ru', 'Fe:Al:Cr:Ni:Ru', 'Fe:Al:Fe:V:Fe', 'Fe:Al:Mn:Al:Co', 'Fe:Co:Fe:Al:Al',
 'Fe:Co:Mo:Ru:Pt', 'Fe:Co:Ni:Al:Zr', 'Fe:Cr:Fe:V:Co', 'Fe:Cr:Mo:V:Re', 'Fe:Cr:Nb:Mo:Pt',
 'Fe:Cr:Ni:V:Al', 'Fe:Cr:Re:Al:Ru', 'Fe:Cr:Ru:Al:Cr', 'Fe:Cr:V:Nb:Mo', 'Fe:Cr:V:Re:Co',
 'Fe:Fe:Al:Co:Mn', 'Fe:Fe:V:Mn:Re', 'Fe:Fe:Zr:Mo:Al', 'Fe:Mn:Fe:Al:Fe', 'Fe:Mn:Mn:Re:Ni',
 'Fe:Mn:Nb:Al:Zr', 'Fe:Mn:Nb:Mo:Al', 'Fe:Mn:W:Ru:V', 'Fe:Mo:Mn:Ni:V', 'Fe:Mo:Mo:V:Ru',
 'Fe:Mo:Ru:Al:Nb', 'Fe:Mo:W:Zr:W', 'Fe:Nb:Cr:Pt:Al', 'Fe:Nb:Fe:Mn:V', 'Fe:Nb:Mo:Mn:Cr',
 'Fe:Nb:Mo:Nb:Ni', 'Fe:Nb:Mo:Re:Ru', 'Fe:Nb:Re:Al:Zr', 'Fe:Nb:Re:V:Mo', 'Fe:Nb:Ru:Nb:Zr',
 'Fe:Ni:Mo:Ni:Fe', 'Fe:Ni:Nb:Al:Pt', 'Fe:Ni:Nb:Ru:Co', 'Fe:Ni:W:Nb:V', 'Fe:Pt:Cr:Al:Mo',
 'Fe:Pt:Fe:Cr:Mn', 'Fe:Pt:V:Fe:Cr', 'Fe:Re:Mn:W:W', 'Fe:Re:Pt:Fe:Al', 'Fe:Ru:Cr:Nb:Re',
 'Fe:Ru:Re:Nb:Mn', 'Fe:Ru:Re:Pt:W', 'Fe:V:Nb:Co:Ru', 'Fe:V:Zr:Fe:W', 'Fe:W:Ni:Mn:Cr',
 'Fe:W:Ni:Zr:Pt', 'Fe:W:Re:Re:Mo', 'Fe:W:W:Re:V', 'Fe:Zr:Nb:Pt:V', 'Mn:Al:Cr:W:Cr',
 'Mn:Al:Ni:Re:Pt', 'Mn:Co:Co:V:Nb', 'Mn:Co:Fe:Al:Mo', 'Mn:Co:Ni:Ru:Co', 'Mn:Co:Pt:Co:W',
 'Mn:Co:V:Pt:Pt', 'Mn:Co:V:V:Fe', 'Mn:Co:W:Fe:Nb', 'Mn:Co:Zr:Mn:Al', 'Mn:Cr:Mn:Fe:V',
 'Mn:Cr:Nb:Ru:Fe', 'Mn:Cr:Ru:Fe:Mo', 'Mn:Cr:V:Re:V', 'Mn:Fe:Cr:Cr:Ru', 'Mn:Fe:Cr:Mn:Al',
 'Mn:Fe:Cr:Zr:Ru', 'Mn:Fe:Mn:Ru:Mn', 'Mn:Fe:Mo:Nb:Re', 'Mn:Fe:Pt:Al:Fe', 'Mn:Fe:Pt:Cr:Fe',
 'Mn:Fe:Re:Al:Al', 'Mn:Mn:Al:Pt:Cr', 'Mn:Mn:Mo:Ru:Fe', 'Mn:Mn:Ni:Ru:Mo', 'Mn:Mn:Ru:Al:Mn',
 'Mn:Mn:Ru:Pt:Ni', 'Mn:Mn:W:Nb:V', 'Mn:Mn:Zr:Re:Ni', 'Mn:Mo:Ru:Pt:Zr', 'Mn:Mo:Ru:Re:Fe',
 'Mn:Mo:Ru:W:Mn', 'Mn:Mo:W:Mn:Mo', 'Mn:Mo:W:Ni:Mo', 'Mn:Nb:Fe:Mn:Re', 'Mn:Nb:Mn:Pt:Fe',
 'Mn:Nb:Mo:Fe:Mo', 'Mn:Nb:V:Fe:Fe', 'Mn:Ni:Al:W:V', 'Mn:Re:Al:Ni:Mn', 'Mn:Re:Mn:Co:Re',
 'Mn:Re:Ni:Mo:Nb', 'Mn:Re:Re:Pt:W', 'Mn:Re:Re:W:Nb', 'Mn:Re:Ru:Co:Ni', 'Mn:Ru:Co:Mo:Ni',
 'Mn:Ru:Nb:Al:Fe', 'Mn:Ru:Re:Cr:Pt', 'Mn:V:Cr:Nb:Al', 'Mn:V:Nb:Pt:W', 'Mn:V:Ru:Ru:Cr',
 'Mn:W:Al:V:Co', 'Mn:W:Co:Pt:Zr', 'Mn:W:Mn:Re:V', 'Mn:W:Ni:Al:Co', 'Mn:W:Zr:Zr:V',
 'Mn:Zr:Al:Mn:V', 'Mn:Zr:Re:V:Nb', 'Mn:Zr:V:Al:Ru', 'Mo:Al:Mn:W:Mn', 'Mo:Al:Nb:Mo:W',
 'Mo:Al:Ni:Co:Ru', 'Mo:Al:Ni:Re:Zr', 'Mo:Al:Ru:Nb:Re', 'Mo:Al:Ru:Nb:Zr', 'Mo:Co:Cr:Mn:Fe',
 'Mo:Co:Nb:Co:Fe', 'Mo:Co:Ru:Al:Zr', 'Mo:Co:Ru:Fe:Ni', 'Mo:Cr:Al:Mn:Zr', 'Mo:Cr:Cr:Ni:W',
 'Mo:Cr:Fe:Re:Mn', 'Mo:Cr:Mn:Fe:Co', 'Mo:Cr:Mo:Mo:Nb', 'Mo:Cr:W:Co:Ni', 'Mo:Fe:Co:Nb:V',
 'Mo:Fe:Cr:Mo:Ni', 'Mo:Fe:Nb:Al:Al', 'Mo:Fe:Ni:Ni:Ni', 'Mo:Fe:Pt:Zr:Nb', 'Mo:Fe:Pt:Zr:Ni',
 'Mo:Mn:Co:Ni:Mo', 'Mo:Mn:Co:W:Nb', 'Mo:Mn:Fe:Cr', 'Mo:Mn:Ni:Mo:Re', 'Mo:Mn:Re:Pt:Ni',
 'Mo:Mn:Zr:V:W', 'Mo:Mo:Al:Co:Fe', 'Mo:Mo:Cr:Mo:Fe', 'Mo:Mo:Cr:V:Mn', 'Mo:Mo:Ni:Nb:Al',
 'Mo:Mo:Ni:W:Mo', 'Mo:Mo:Re:Al:Zr', 'Mo:Mo:W:Al:Pt', 'Mo:Nb:Nb:Fe:Co', 'Mo:Ni:Cr:Fe:Mn',
 'Mo:Ni:Fe:Ni:Mn', 'Mo:Ni:Nb:Nb:Cr', 'Mo:Ni:Nb:Re:Pt', 'Mo:Ni:W:Ni:Nb', 'Mo:Pt:Co:W:Nb',
 'Mo:Pt:Pt:Re:Zr', 'Mo:Re:Cr:Zr:Re', 'Mo:Re:Mn:Co:Al', 'Mo:Re:Pt:W:V', 'Mo:Re:Ru:Al:Re',
 'Mo:Re:Ru:V:Fe', 'Mo:Re:V:Fe:Fe', 'Mo:Re:V:Re:Pt', 'Mo:Re:V:W:Nb', 'Mo:Ru:Al:Fe:Al',

'Mo:Ru:Al:Re:V', 'Mo:Ru:Co:Re:Ni', 'Mo:Ru:Cr:Pt:Ni', 'Mo:Ru:Ni:Ni:Fe', 'Mo:Ru:Ru:W:Zr',
 'Mo:V:Pt:Ni:Nb', 'Mo:V:V:Ru:Ru', 'Mo:V:W:Re:Al', 'Mo:V:W:Zr:Co', 'Mo:W:Cr:Ru:Nb',
 'Mo:W:Re:Zr:Cr', 'Mo:W:V:Ni:Fe', 'Mo:Zr:Al:Nb:Co', 'Mo:Zr:Fe:Nb:Pt', 'Mo:Zr:Fe:Ni:Pt',
 'Mo:Zr:Mo:V:W', 'Mo:Zr:Ni:Pt:Fe', 'Mo:Zr:Pt:Co:Ru', 'Mo:Zr:Re:Fe:Ni', 'Mo:Zr:Re:Mn:Nb',
 'Mo:Zr:V:Pt:Cr', 'Mo:Zr:V:V:Fe', 'Nb:Al:Co:Ni:Cr', 'Nb:Al:Re:Ni:Cr', 'Nb:Al:Ru:Mo:Re',
 'Nb:Co:Ni:Co:Pt', 'Nb:Co:Ni:Fe:Fe', 'Nb:Co:Zr:Co:Cr', 'Nb:Cr:Cr:Zr:Pt', 'Nb:Cr:Mn:Pt:Pt',
 'Nb:Cr:Nb:Ni:Co', 'Nb:Cr:Re:Pt:Ni', 'Nb:Fe:Co:Al:Re', 'Nb:Fe:Mn:Mo:Mo', 'Nb:Fe:Nb:Pt:W',
 'Nb:Fe:V:Pt:V', 'Nb:Fe:Zr:Ni:Co', 'Nb:Mn:Cr:Pt:Al', 'Nb:Mn:Fe:V:Pt', 'Nb:Mn:Re:Nb:Nb',
 'Nb:Mn:Zr:Nb:V', 'Nb:Mo:Fe:Zr:Mo', 'Nb:Mo:Ru:W:Fe', 'Nb:Mo:Zr:Co:Co', 'Nb:Nb:Co:Ru:Al',
 'Nb:Nb:Nb:Mn:Re', 'Nb:Nb:Re:Ni:V', 'Nb:Nb:Zr:Re:Nb', 'Nb:Ni:Cr:Ru:Fe', 'Nb:Ni:Fe:Mo:Pt',
 'Nb:Ni:Mn:Zr:Mo', 'Nb:Ni:V:Ni:Co', 'Nb:Pt:Ni:Co:Re', 'Nb:Pt:Ru:Al:Fe', 'Nb:Re:Al:Fe:Fe',
 'Nb:Re:Co:Nb:Al', 'Nb:Re:Co:Pt:Ru', 'Nb:Re:Co:W:Mn', 'Nb:Re:Nb:W:Ru', 'Nb:Re:Pt:Nb:Nb',
 'Nb:Re:W:Nb:Mn', 'Nb:Re:W:Nb:Pt', 'Nb:Ru:Co:Mn:Ru', 'Nb:Ru:Cr:Nb:Re', 'Nb:Ru:Nb:Ni:V',
 'Nb:Ru:W:Re:Pt', 'Nb:V:Mn:Pt:Fe', 'Nb:V:Nb:Zr:Al', 'Nb:V:Re:Mo:V', 'Nb:V:Ru:Nb:Nb',
 'Nb:W:Ni:Zr:Nb', 'Nb:W:Re:Ru:Al', 'Nb:W:V:V:Mn', 'Nb:Zr:Co:Ru:W', 'Nb:Zr:Mo:Ni:Ni',
 'Nb:Zr:Mo:Pt:Fe', 'Nb:Zr:Mo:Re:Fe', 'Nb:Zr:Ni:Ni:Pt', 'Nb:Zr:Re:Mn:Mo', 'Nb:Zr:Ru:W:Re',
 'Nb:Zr:V:Nb:Co', 'Nb:Zr:W:Ni:Zr', 'Nb:Zr:Zr:Ru:W', 'Ni:Al:Cr:Ni:Zr', 'Ni:Al:Cr:Re:Pt',
 'Ni:Al:Cr:W:Nb', 'Ni:Co:Co:Co:Ru', 'Ni:Co:Co:Cr:Pt', 'Ni:Co:Cr:Cr:Cr', 'Ni:Co:Fe:Al:V',
 'Ni:Co:Nb:W:Mn', 'Ni:Co:Ni:Al:V', 'Ni:Co:Pt:Zr:Nb', 'Ni:Co:Ru:Zr:Nb', 'Ni:Co:V:Ni:Ru',
 'Ni:Co:Zr:Ni:Ni', 'Ni:Co:Zr:Re:Ru', 'Ni:Cr:Co:W:W', 'Ni:Cr:Nb:Nb:Fe', 'Ni:Cr:Ni:Nb:Pt',
 'Ni:Cr:Re:Re:Ni', 'Ni:Cr:Ru:Cr:Re', 'Ni:Cr:Zr:Nb:Ru', 'Ni:Fe:Co:W:Pt', 'Ni:Fe:Mo:Cr:Zr',
 'Ni:Fe:Ni:Pt:Fe', 'Ni:Fe:Pt:Cr:Pt', 'Ni:Fe:W:Cr:Ru', 'Ni:Fe:W:Mn:Mo', 'Ni:Fe:Zr:Mn:Nb',
 'Ni:Mn:Re:Cr:W', 'Ni:Mn:V:Zr:Nb', 'Ni:Mo:Mn:W:W', 'Ni:Mo:Nb:W:V', 'Ni:Mo:Ni:Mo:Mn',
 'Ni:Mo:Ni:Ni:Ni', 'Ni:Mo:Zr:Co:W', 'Ni:Nb:Mo:Pt:Mn', 'Ni:Nb:Re:Co:V', 'Ni:Nb:Re:Mn:Mn',
 'Ni:Nb:V:Pt:W', 'Ni:Ni:Ni:V:Re', 'Ni:Ni:V:Ru:Nb', 'Ni:Pt:Al:Mn:Zr', 'Ni:Pt:Co:Al:V',
 'Ni:Pt:Fe:Ni:Mn', 'Ni:Pt:Mn:Cr:Nb', 'Ni:Pt:Ru:Al:Ru', 'Ni:Pt:V:Mn:Co', 'Ni:Re:Fe:Pt:Ni',
 'Ni:Re:Fe:Ru:Fe', 'Ni:Ru:Al:Co:Mo', 'Ni:Ru:Co:Ru:Ru', 'Ni:Ru:Mn:Re:Zr', 'Ni:Ru:Mo:Pt:Ni',
 'Ni:Ru:Ru:Zr:Fe', 'Ni:Ru:V:Ni:Mo', 'Ni:Ru:Zr:Fe:Cr', 'Ni:V:Mn:Re:Mo', 'Ni:V:Mn:V:Pt',
 'Ni:V:Pt:Cr:Pt', 'Ni:V:Pt:Ru:W', 'Ni:V:W:Re:Re', 'Ni:W:Al:Cr:Mo', 'Ni:W:Cr:Ru:Zr',
 'Ni:W:Fe:V:V', 'Ni:W:Ni:Zr:Zr', 'Ni:W:Pt:V:Fe', 'Ni:W:Re:Mn:Mn', 'Ni:W:W:Mn:Mo',
 'Ni:W:W:Mo:V', 'Ni:Zr:Cr:Cr:Zr', 'Ni:Zr:Mo:Cr:Zr', 'Ni:Zr:W:Ni:Co', 'Pt:Al:Al:Re:Pt',
 'Pt:Al:Fe:Mn:Cr', 'Pt:Al:Ni:Mo:V', 'Pt:Al:Pt:Ru:Zr', 'Pt:Al:Ru:Fe:Ru', 'Pt:Al:V:Nb:Nb',
 'Pt:Co:Mn:Nb:Mn', 'Pt:Co:Nb:Co:Re', 'Pt:Co:V:W:Al', 'Pt:Co:W:Nb:Nb', 'Pt:Co:Zr:Mo:V',
 'Pt:Cr:Al:Nb:Re', 'Pt:Cr:Fe:Cr:Nb', 'Pt:Cr:Mn:Mo:Co', 'Pt:Cr:Nb:Mo:Pt', 'Pt:Cr:Pt:Ru:Cr',
 'Pt:Cr:Re:Mn:Fe', 'Pt:Cr:W:Re:Al', 'Pt:Cr:Zr:W:Al', 'Pt:Fe:Fe:Cr:Cr', 'Pt:Fe:Fe:Fe:Pt',
 'Pt:Fe:Mo:V:Fe', 'Pt:Mn:Cr:Ni:Ni', 'Pt:Mn:Mo:W:Mo', 'Pt:Mn:Nb:Co:Pt', 'Pt:Mn:Nb:W:V',
 'Pt:Mn:Re:Pt:Cr', 'Pt:Mn:W:Al:Nb', 'Pt:Mo:Nb:Co:Al', 'Pt:Mo:Nb:Re:Pt', 'Pt:Mo:Ru:W:Ru',
 'Pt:Mo:Zr:Co:W', 'Pt:Nb:Al:Nb:Ni', 'Pt:Nb:Pt:Cr:Mo', 'Pt:Nb:Pt:Ni:Al', 'Pt:Nb:Ru:Cr:Ni',
 'Pt:Ni:Ni:Mn:W', 'Pt:Ni:Ni:Ni:Ru', 'Pt:Pt:Re:Mn:Nb', 'Pt:Re:Mn:Fe:Al', 'Pt:Re:Re:Zr:V',
 'Pt:Re:Ru:Co:Re', 'Pt:Re:V:Mn:Re', 'Pt:Re:W:V:W', 'Pt:Re:Zr:Mo:Co', 'Pt:Ru:Al:Ni:Mn',
 'Pt:Ru:Cr:Al:Cr', 'Pt:Ru:Cr:Mn:Co', 'Pt:Ru:Mn:Fe:Re', 'Pt:Ru:Mn:V:Nb', 'Pt:V:Al:Pt:Zr',
 'Pt:V:Fe:Pt:Pt', 'Pt:V:Mn:Re:Ni', 'Pt:V:Re:W:Pt', 'Pt:V:V:Mn:Mo', 'Pt:W:Al:Cr:V',
 'Pt:W:Mo:Ni:Re', 'Pt:W:Re:Fe:Mn', 'Pt:Zr:Al:Mo:Nb', 'Pt:Zr:Co:Mn:Fe', 'Pt:Zr:Fe:Fe:V',
 'Pt:Zr:Nb:W:Pt', 'Pt:Zr:Re:Nb:Pt', 'Pt:Zr:Ru:W:Ru', 'Re:Al:Co:Fe:Cr', 'Re:Al:Cr:Zr:Ru',
 'Re:Al:Fe:Mo:Co', 'Re:Al:Mn:Ru:Cr', 'Re:Al:Nb:Pt:V', 'Re:Al:V:Mn:W', 'Re:Co:Cr:V:Co',
 'Re:Co:Mo:Re:Co', 'Re:Co:Mo:Ru:Nb', 'Re:Co:Pt:Co:Nb', 'Re:Co:Re:Re:Pt', 'Re:Co:V:Ru:Ni',

'Re:Cr:Al:Co:Ni', 'Re:Cr:Al:W:Al', 'Re:Cr:Co:Cr:Cr', 'Re:Cr:Ni:Mn:Re', 'Re:Fe:Mn:Mn:Al',
 'Re:Fe:Ni:Ru:Nb', 'Re:Fe:Pt:V:Re', 'Re:Fe:Re:Co:Zr', 'Re:Fe:Ru:Mn:Ni', 'Re:Fe:Zr:Fe:Mn',
 'Re:Mn:Mn:Mo:Nb', 'Re:Mn:Re:Cr:Pt', 'Re:Mn:Re:Pt:Pt', 'Re:Mo:Al:Re:Nb', 'Re:Mo:Cr:Mn:Cr',
 'Re:Mo:Nb:Co:Ru', 'Re:Mo:Pt:Ru:Nb', 'Re:Mo:Pt:Ru:Ni', 'Re:Mo:Ru:W:Pt', 'Re:Nb:Mn:Ru:Fe',
 'Re:Nb:Nb:Re:Al', 'Re:Nb:Pt:W:Pt', 'Re:Ni:Mo:W:Re', 'Re:Ni:Ni:Mn:Nb', 'Re:Ni:Pt:Nb:Re',
 'Re:Ni:Pt:V:Fe', 'Re:Ni:Pt:V:Ru', 'Re:Ni:Re:Fe:Zr', 'Re:Ni:W:Cr:Cr', 'Re:Pt:Cr:Nb:Fe',
 'Re:Pt:Mn:Ni:Co', 'Re:Pt:Nb:Nb:Pt', 'Re:Pt:Ni:Re:Co', 'Re:Pt:V:Re:Zr', 'Re:Pt:W:Pt:Nb',
 'Re:Re:Fe:Re:Cr', 'Re:Re:Pt:Mo:Re', 'Re:Ru:Cr:Fe:Al', 'Re:Ru:Mo:Cr:Fe', 'Re:Ru:Pt:Mo:Co',
 'Re:Ru:Pt:Nb:Ru', 'Re:Ru:Pt:Pt:W', 'Re:V:Mn:Pt:Re', 'Re:V:Ni:Co:Zr', 'Re:V:Re:Ru:Co',
 'Re:V:Re:Zr:Mo', 'Re:V:V:Co:Fe', 'Re:V:Zr:Co:Mn', 'Re:W:Cr:Mn:Re', 'Re:W:Nb:Al:Fe',
 'Re:W:Ni:Re:Nb', 'Re:W:Ru:Fe:Fe', 'Re:W:V:Fe:Zr', 'Re:W:W:Co:Ni', 'Re:W:Zr:Nb:Ni',
 'Re:Zr:Co:Cr:Ni', 'Re:Zr:Co:Zr:Fe', 'Re:Zr:Cr:Co:Co', 'Re:Zr:Mo:Pt:Mn', 'Re:Zr:Nb:Ru:Cr',
 'Re:Zr:Ni:Zr:Pt', 'Re:Zr:Pt:Nb:Re', 'Re:Zr:Pt:Nb:W', 'Re:Zr:Ru:W:W', 'Re:Zr:W:Cr:Zr',
 'Ru:Al:Cr:W:Nb', 'Ru:Co:Fe:Al:Mn', 'Ru:Co:W:Pt:Pt', 'Ru:Cr:Co:W:Ni', 'Ru:Cr:Cr:Cr:Mo',
 'Ru:Cr:Nb:Cr:Mo', 'Ru:Cr:Ni:Nb:Ru', 'Ru:Cr:Ni:V:Pt', 'Ru:Cr:Pt:Mn:Nb', 'Ru:Cr:Ru:Ru:Ru',
 'Ru:Cr:V:Mn:Mn', 'Ru:Cr:V:V:Nb', 'Ru:Cr:Zr:Al:Pt', 'Ru:Cr:Zr:Co:Pt', 'Ru:Fe:Co:W:Mo',
 'Ru:Fe:Mn:Nb:Pt', 'Ru:Fe:Mo:Zr:Co', 'Ru:Fe:Re:Cr:Zr', 'Ru:Fe:Re:Fe:Pt', 'Ru:Mn:Cr:Cr:Al',
 'Ru:Mn:Cr:Mo:Al', 'Ru:Mn:Cr:Ru:W', 'Ru:Mn:Fe:W:Ru', 'Ru:Mo:Co:Zr:Nb', 'Ru:Mo:Mo:Ru:W',
 'Ru:Mo:Nb:Mo:Zr', 'Ru:Mo:Pt:Re:Al', 'Ru:Mo:Re:Fe:Mn', 'Ru:Mo:Re:Mn:Al', 'Ru:Mo:Ru:W:Mo',
 'Ru:Mo:Zr:Co:Nb', 'Ru:Nb:Al:Re:Co', 'Ru:Nb:Fe:Cr:Pt', 'Ru:Nb:Fe:Mo:Fe', 'Ru:Nb:Mo:Fe:Mo',
 'Ru:Nb:Re:Mo:Pt', 'Ru:Nb:V:W:W', 'Ru:Ni:Cr:Mn:Nb', 'Ru:Ni:Mo:Mo:Fe', 'Ru:Ni:Ni:Pt:Mo',
 'Ru:Ni:Ru:Cr:V', 'Ru:Ni:V:Zr:Al', 'Ru:Pt:Al:V:Co', 'Ru:Pt:Cr:Co:Pt', 'Ru:Pt:Ni:Mo:Ru',
 'Ru:Pt:Re:V:Zr', 'Ru:Pt:Ru:W:W', 'Ru:Pt:W:Re:Ni', 'Ru:Pt:Zr:Co:Zr', 'Ru:Re:Cr:Mo:Nb',
 'Ru:Re:Fe:Fe:Zr', 'Ru:Re:Fe:Ru:Nb', 'Ru:Re:Fe:Zr:W', 'Ru:Re:Nb:Co:Cr', 'Ru:Re:Re:Re:Nb',
 'Ru:Ru:Mo:Pt:Cr', 'Ru:Ru:Nb:Mn:V', 'Ru:Ru:Re:W:Co', 'Ru:Ru:Ru:W:Re', 'Ru:Ru:W:Mo:Pt',
 'Ru:Ru:W:Ni:Ni', 'Ru:V:Cr:Mo:Mn', 'Ru:V:W:Re:Zr', 'Ru:V:Zr:Mo:Cr', 'Ru:W:Cr:Cr:Mo',
 'Ru:W:Ru:Fe:Fe', 'Ru:Zr:Cr:Nb:Pt', 'Ru:Zr:Fe:Fe:W', 'Ru:Zr:Fe:Ni:V', 'Ru:Zr:Nb:Fe:Pt',
 'Ru:Zr:Ni:Fe:Ru', 'Ru:Zr:Ni:Re:Nb', 'V:Al:Mo:V:Al', 'V:Al:Nb:Cr:W', 'V:Al:Ni:V:Mo',
 'V:Co:Co:Re:Zr', 'V:Cr:Cr:Co:V', 'V:Cr:Cr:Zr:Cr', 'V:Cr:Mn:Mo:Pt', 'V:Cr:Pt:V:Fe',
 'V:Fe:Co:Re:Al', 'V:Fe:Cr:Pt:W', 'V:Fe:Fe:Al:W', 'V:Fe:Nb:Ru:Mo', 'V:Fe:Re:Ni:Zr',
 'V:Mn:Co:Fe:Co', 'V:Mn:Co:Fe:Nb', 'V:Mn:Mo:Ni:Ni', 'V:Mn:Ru:Pt:Fe', 'V:Mn:V:Ni:V',
 'V:Mo:Ni:Fe:Nb', 'V:Mo:Pt:W:W', 'V:Mo:W:Al:Mo', 'V:Mo:Zr:Fe:Ni', 'V:Nb:Cr:Al:Cr',
 'V:Nb:Mn:Al:Al', 'V:Nb:Re:Cr:Re', 'V:Nb:Ru:V:Ni', 'V:Ni:Al:Pt:Fe', 'V:Ni:Al:W:Co',
 'V:Ni:Ni:Co:V', 'V:Ni:V:V:Ni', 'V:Ni:W:Re:Fe', 'V:Pt:Co:Co:Pt', 'V:Pt:Co:Mn:Re',
 'V:Pt:Co:Ru:V', 'V:Pt:Pt:Fe:V', 'V:Pt:Re:Ni:Ru', 'V:Pt:Zr:Co:Pt', 'V:Re:Al:Cr:Ni',
 'V:Re:Cr:Ru:Pt', 'V:Re:Ru:Mo:Co', 'V:Re:Ru:Zr:W', 'V:Re:Zr:Pt:Ru', 'V:Ru:Co:Co:Pt',
 'V:Ru:Co:Pt:Zr', 'V:Ru:Mn:Mn:Re', 'V:Ru:Nb:Al:Ru', 'V:Ru:Nb:Pt:Fe', 'V:Ru:Ni:Ru:Ru',
 'V:Ru:V:Mn:Ni', 'V:V:Co:Pt:Pt', 'V:V:Cr:W:Re', 'V:V:Mn:Mn:Mn', 'V:V:Mn:V:Ni',
 'V:V:Nb:V:Co', 'V:V:Ni:Fe:Al', 'V:W:Mo:Nb:Zr', 'V:Zr:Mn:W:Nb', 'V:Zr:Ni:Nb:Zr',
 'V:Zr:Ru:Cr:Nb', 'V:Zr:Ru:W:Co', 'V:Zr:Zr:Cr:Al', 'W:Al:Ru:Nb:Cr', 'W:Al:V:Nb:Mo',
 'W:Al:V:Ru:Pt', 'W:Al:Zr:Nb:Ni', 'W:Co:Al:Mn:Cr', 'W:Co:V:Pt:Pt', 'W:Co:W:Ru:Co',
 'W:Co:Zr:Fe:Pt', 'W:Cr:Ni:Ni:Mo', 'W:Cr:Zr:Mn:Fe', 'W:Cr:Zr:V:Ni', 'W:Fe:Ni:Mo:W',
 'W:Fe:Ni:Re:Mo', 'W:Fe:V:Mn:Pt', 'W:Mn:Mn:Mo:Zr', 'W:Mn:Nb:Ru:Ni', 'W:Mn:Pt:Nb:Nb',
 'W:Mn:V:Cr:Fe', 'W:Mn:V:Fe:V', 'W:Mo:Cr:Al:Fe', 'W:Mo:Mo:Pt:Al', 'W:Mo:Nb:W:Mn',
 'W:Mo:Re:Mn:Cr', 'W:Mo:Zr:Re:Ru', 'W:Nb:Fe:Co:Al', 'W:Nb:Ni:V:Fe', 'W:Nb:Re:Ru:Re',
 'W:Nb:Ru:Al:Ni', 'W:Nb:Ru:Cr:V', 'W:Ni:Al:Al:Mo', 'W:Ni:Co:V:Re', 'W:Ni:Cr:Pt:Ni',

'W:Ni:Cr:Zr:Pt', 'W:Ni:Mn:Al:W', 'W:Ni:Pt:Ni:Ru', 'W:Pt:Cr:Ru:Mo', 'W:Pt:Ni:Ru:Al',
 'W:Pt:Ru:Fe:Ru', 'W:Pt:W:Al:Al', 'W:Re:Cr:Fe:Fe', 'W:Re:Fe:Re:Cr', 'W:Re:Mn:W:Mo',
 'W:Re:Mo:Co:Ni', 'W:Re:Nb:Co:Re', 'W:Re:Pt:Pt:Cr', 'W:Re:Zr:Re:Mn', 'W:Ru:Nb:Zr:Pt',
 'W:V:Co:Fe:Fe', 'W:V:Cr:V:Mn', 'W:V:Fe:V:Mn', 'W:V:Nb:Al:Nb', 'W:V:Ni:V:V',
 'W:V:Ru:Al:Zr', 'W:V:Ru:Re:Mo', 'W:V:Zr:Ru:Ni', 'W:W:Co:Cr:Nb', 'W:W:Co:Mn:W',
 'W:W:Ni:Mo:Ni', 'W:W:Re:Zr:Nb', 'W:W:V:Mo:Ru', 'W:W:V:Zr:Nb', 'W:Zr:Co:Mn:Mn',
 'W:Zr:Nb:Ni:Mo', 'W:Zr:Re:Nb:Ru', 'W:Zr:Ru:Mn:Ni', 'W:Zr:W:Mn:Re', 'W:Zr:W:V:Zr',
 'Zr:Al:Mo:Ru:Mn', 'Zr:Al:Nb:Cr:Pt', 'Zr:Al:Ni:Zr:W', 'Zr:Al:Ru:Pt:Pt', 'Zr:Co:Mo:V:Pt',
 'Zr:Co:Ni:Mo:Pt', 'Zr:Co:Pt:V:Nb', 'Zr:Co:Re:Pt:V', 'Zr:Cr:Mo:Mo:Cr', 'Zr:Cr:Re:Ni:Re',
 'Zr:Cr:Ru:Ru:Pt', 'Zr:Cr:V:Pt:Fe', 'Zr:Cr:Zr:Zr:Pt', 'Zr:Fe:Ni:Mo:Al', 'Zr:Mn:Al:Fe:W',
 'Zr:Mn:Co:Mn:Mn', 'Zr:Mn:Nb:Ru:Ni', 'Zr:Mn:Nb:Ru:Pt', 'Zr:Mn:Ni:Nb:Cr', 'Zr:Mo:Fe:Fe:Mn',
 'Zr:Mo:Pt:Al:Cr', 'Zr:Nb:Mo:Fe:Co', 'Zr:Nb:Re:Cr:Ru', 'Zr:Nb:W:Al:Co', 'Zr:Ni:Mo:Mn:Fe',
 'Zr:Ni:W:Fe:Ru', 'Zr:Pt:Cr:Fe:Cr', 'Zr:Pt:Cr:Nb:Al', 'Zr:Pt:Nb:Co:Fe', 'Zr:Pt:W:W:Pt',
 'Zr:Re:Co:Al:Zr', 'Zr:Re:Mn:W:Cr', 'Zr:Re:Re:V:Mo', 'Zr:Ru:Cr:Pt:Ru', 'Zr:Ru:Fe:Zr:Nb',
 'Zr:Ru:Mn:Cr:Ni', 'Zr:Ru:Mo:Ni:Nb', 'Zr:V:Co:Mo:W', 'Zr:V:Co:Re:W', 'Zr:V:Mn:Re:Al',
 'Zr:V:Ni:Cr:Mo', 'Zr:V:Re:Pt:Cr', 'Zr:W:Mn:Fe:Al', 'Zr:W:Mo:Mo:V', 'Zr:W:Ni:Re:Cr',
 'Zr:W:Re:Re:Co', 'Zr:W:Zr:Al:Ni', 'Zr:Zr:Al:Co:Cr', 'Zr:Zr:Fe:Co:Zr', 'Zr:Zr:Mn:Cr:Pt',
 'Zr:Zr:Re:Co:W', 'Zr:Zr:Ru:Co:Mo', 'Zr:Zr:V:Zr:Al', 'Zr:Zr:W:W:Zr', 'Zr:Zr:Zr:Al:Ru',
 'Zr:Zr:Zr:Co:Mo',

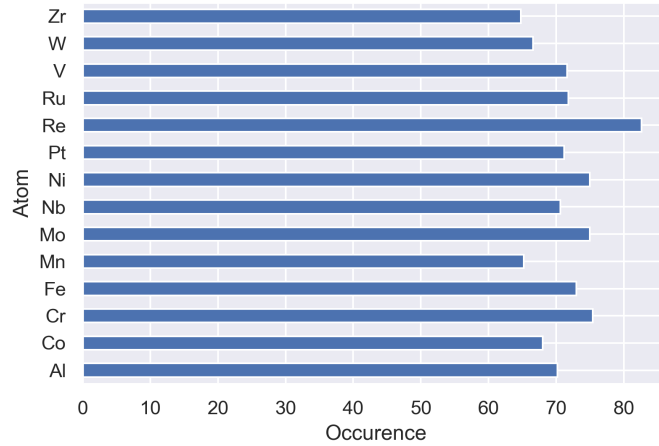


FIG. 11: Occurrence of the $n = 14$ elements in the testing database (1001 entries).

Appendix F: Prediction from several simulations of training and testing sets

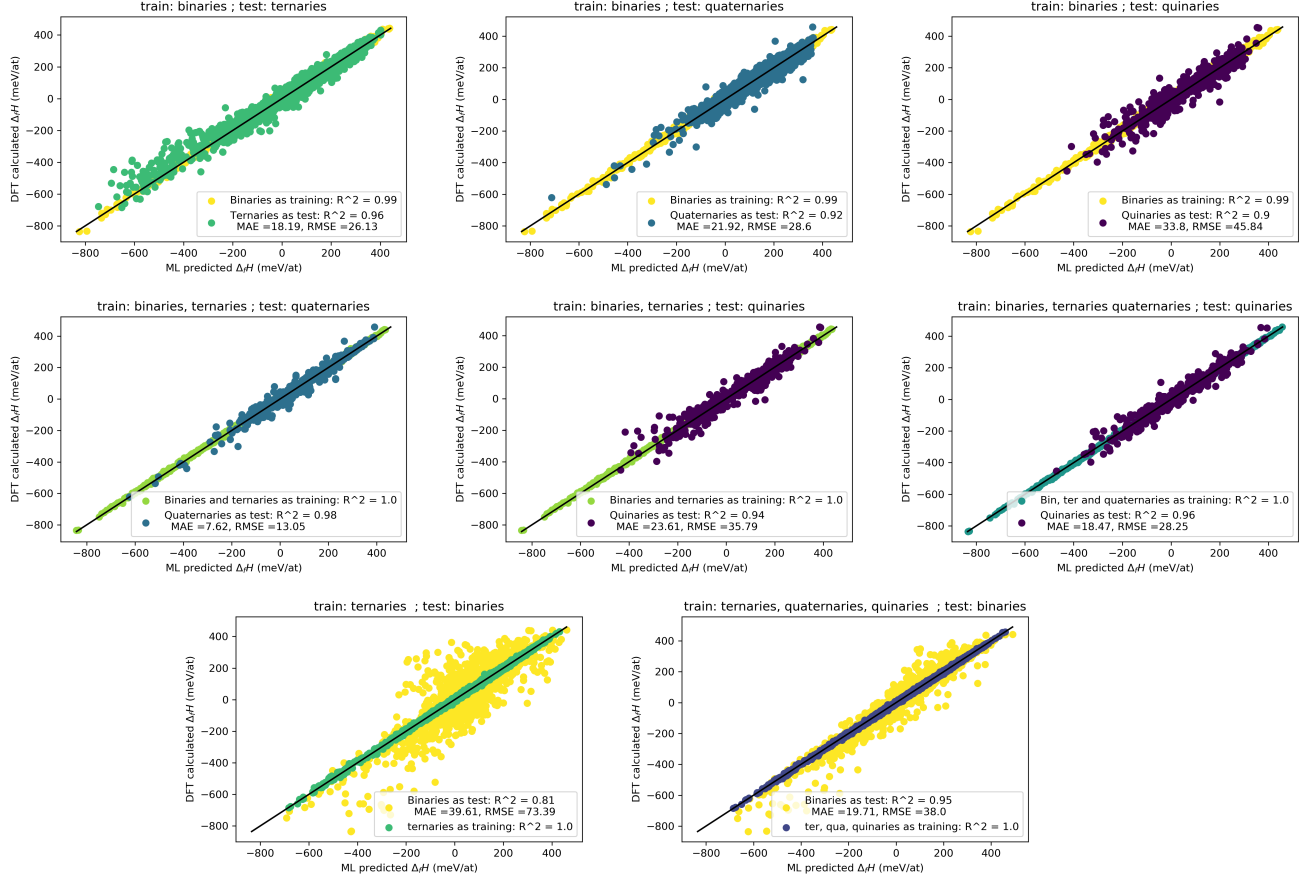


FIG. 12: Simulation of the prediction with MPR from several proportions of training and testing sets including binaries (yellow), ternaries (green), quaternaries (blue) or quinaries (dark purple). The diagonal line indicates the perfect agreement between predicted and real values.

Appendix G: Influence of additional featuring

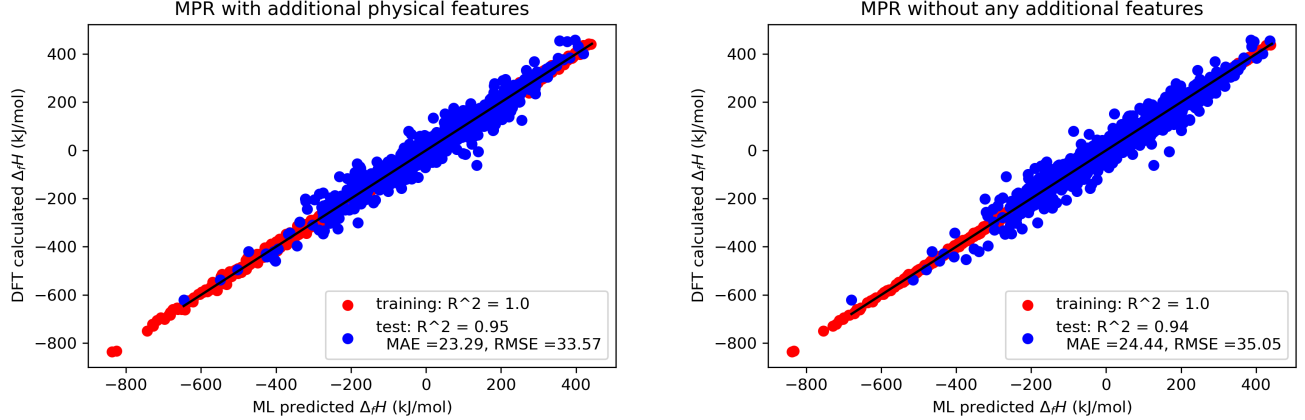


FIG. 13: Prediction with MPR of the randomized set from the learning database with (right) and without (left) additional featuring (atomic radius and number of valence electrons). The diagonal line indicates the perfect agreement between calculated and predicted values.

Appendix H: Results of prediction of every 14^5 configurations

All of the data, including heat of formation ($\Delta_f H$), cell parameters (a, c) and 7 internal parameters ($x^{4f}, x^{8i_1}, y^{8i_1}, x^{8i_2}, y^{8i_2}, x^{8j}, z^{8j}$), generated for the $14^5 = 537,824$ configurations in this study are available from the authors on request.

Appendix I: Prediction of σ -phase crystal parameters

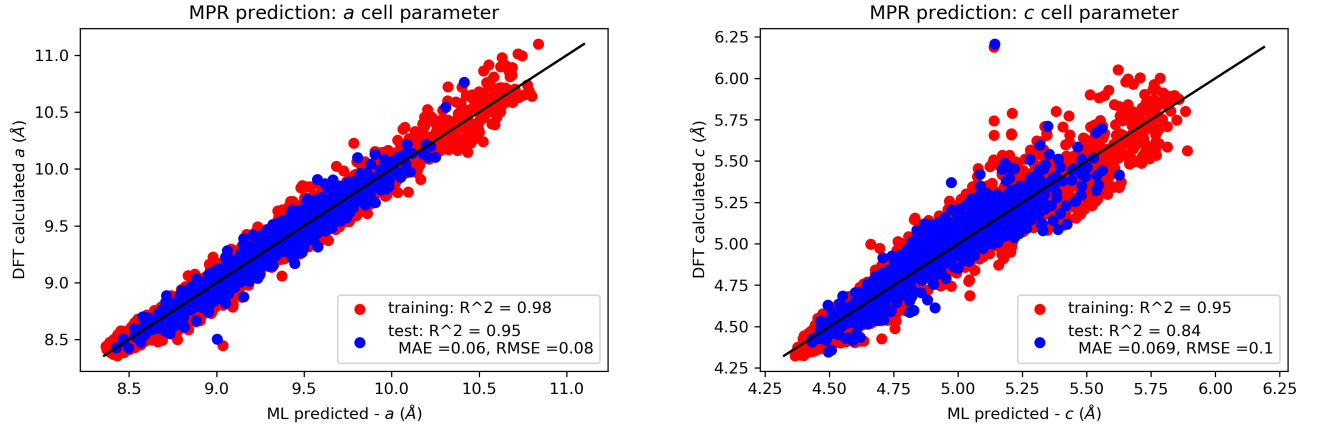


FIG. 14: Prediction of both a and c tetragonal cell parameters of randomized 1001 testing configurations from the MPR learning of the training database (9974 data in red).

Appendix J: DFT calculation methodology

The Density Functional Theory (DFT) method has been used to perform the electronic structure calculations.^{42,43} As implemented in the Vienna *Ab initio* Simulation Package (VASP), the Projector Augmented Wave (PAW) pseudo-potentials method was used.^{44–47} Exchange and correlations were considered in the Generalized Gradient Approximation (GGA) with the Perdew-Burke-Ernzerhof (PBE) functional.^{48,49} Convergence tests were performed with respect to the number of plane waves and the \mathbf{k} -points mesh. The self-consistent total energy calculations converged to less than 0.01 meV, with a 400 eV cutoff energy and with \mathbf{k} -points spacing less than 0.06 \AA^{-1} in each direction, samplings generated by the Monkhorst-Pack procedure (10x10x10 points in the irreducible wedge of the Brillouin zone).⁵⁰. For all the $9974 + 1001 = 10,975$ configurations, both the lattice parameters and internal atomic coordinates were fully relaxed by several intermediate steps, within a residual Hellmann-Feynman force of less than 5 meV/ \AA . Total energies have been calculated using the linear tetrahedron method with Blöchl corrections⁵¹. The magnetism was not yet considered since routine calculations with spin polarization are not robust but are necessary for a correct energy prediction and will be considered in an future work. The heat of formation, $\Delta_f H$, of a given $i:j:k:l:m$ configuration is given by the difference of its total DFT energy related to the element energies in their stable reference state (SER). Additional tools, such as Vesta and Phonopy, for crystal representation and for checking relaxed structure symmetry were used.^{52,53}

Contents

I. Introduction	2
II. Results	3
A. General-purpose method	4
B. Prediction of the heat of formation	5
C. Validation of learned models on an independent validation set	6
III. Discussion	7
A. Influence of the system degree	7
B. Contribution of additional descriptors	9
C. Prediction of crystal properties	9
D. Conclusions and outlook	10
IV. Methods	11
A. Training database from DFT calculations	11
B. Database construction format	11
C. Estimation of the machine learning models	12
Data and code availability	15
Acknowledgements	16
Author contributions	16
Competing Interests	16
Additional Information	16
References	16
References	16
A. Crystal details of the σ-phase	22
B. Analysis of the combinatorial descriptions	23

C. The training database, 9974 configurations	24
1. List of systems included in the training database	24
2. Statistical analysis of the training database	26
D. Cross validation results from the only training database	28
E. List of the 1001 testing set configurations	29
F. Prediction from several simulations of training and testing sets	34
G. Influence of additional featuring	35
H. Results of prediction of every 14^5 configurations	35
I. Prediction of σ-phase crystal parameters	36
J. DFT calculation methodology	37